

Electronic supplementary information for:

Stepwise Assembly of Heteroleptic, Heterometallic “Triblock Janus-type” Metal-Organic Polyhedra

Cornelia von Baeckmann,^{a,b} Sara Ruiz-Relaño,^{a,b} Inhar Imaz,^{a,b} Marcel Handke,^{a,b} Judith Juanhuix,^c Felipe Gándara,^d Arnau Carné-Sanchez,^{a,b,*} and Daniel Maspoch^{a,b,e,*}

- a. *Catalan Institute of Nanoscience and Nanotechnology (ICN2), CSIC, and The Barcelona Institute of Science and Technology, Campus UAB, Bellaterra, 08193 Barcelona, Spain*
- b. *Departament de Química, Facultat de Ciències Universitat Autònoma de Barcelona, 08193 Bellaterra, Spain*
- c. *Alba Synchrotron Light Facility, Cerdanyola del Vallès, 08290 Barcelona, Spain*
- d. *Materials Science Institute of Madrid (ICMM), Consejo Superior de Investigaciones Científicas (CSIC), Calle Sor Juana Inés de la Cruz, 3, 28049 Madrid, Spain*
- e. *ICREA, Pg. Lluís Companys 23, 08010 Barcelona, Spain*

Table of contents

S1. Materials and methods

S1.1 Materials and characterization

S1.2 Crystallography

S1.3. Synthetic procedures

S2. Characterization of organic linkers

S3. Characterization of $\text{Rh}_2(\text{bdc})_4$ complexes

S4. Characterization of HET-MOP-1

S5. Characterization of HET-MOP-2

S6. Characterization of HET-MOP-3

S1. Materials and methods

S1.1 Materials and characterization

Isophthaloyl chloride, isophthalic acid (bdc), 5-hydroxyisophthalic acid (OH-bdc), 5-sulfoisophthalic acid sodium salt (NaSO₃-bdc), tetrabutylammonium fluoride solution (1M in THF), pyridine, 4-tert-butylpyridine and chlorobenzene were obtained from Sigma-Aldrich in high purity grade. 2-(Trimethylsilyl)ethanol (TMS-OH) was purchased from TCI. DMSO-d₆ and CDCl₃ were obtained from euroisotop, rhodium(II) acetate dimer and deuterium chloride (DCI, 20wt% in D₂O) from Acros Organics. Dichloromethane (DCM), diethyl ether (Et₂O), tetrahydrofuran (THF), N,N-dimethylacetamide (DMA), dimethylformamide (DMF), hexane, ethylacetate (EtOAc) and methanol (MeOH) were used without any further purification from Fisher Scientific.

Nuclear magnetic resonance (NMR). All ¹H NMR and ¹³C NMR spectra were recorded using a Bruker Avance NEO 300 NMR spectrometer at 25 °C. Chemical shifts (δ) are reported in ppm and coupling constants (J) in Hz. The resonance of residual CHCl₃ for CDCl₃ (7.26 ppm) and DMSO for DMSO-d₆ (2.5 ppm) is used as internal reference. ¹H NMR splitting patterns were indicated as singlet (s), doublet (d), triplet (t) and multiplet (m). All reagents were used as obtained by the suppliers, unless it is stated otherwise.

Matrix-assisted laser desorption/ionization-time of flight (MALDI-TOF) mass spectrometry (MS) measurements were performed using a 4800 Plus MALDI TOF/TOF (ABSCIEX – 2010) operating in positive-ionization mode using trans-2-[3-(4-tert-butylphenyl)-2-methyl-2-propenyldene]malononitrile (DCTB) as ionization matrix.

Electrospray ionization time-of-flight (ESI-TOF) mass spectrometry (MS) measurements were performed using a LC/MSD-TOF (Agilent Technologies, G1969A) operating in negative-ionization mode.

Scanning Electron Microscopy-Energy Dispersive X-ray spectroscopy (SEM-EDX) was performed in a SEM Quanta 650 FEM and SEM Magellan 400L XHR.

Ultraviolet-visible (UV-Vis) spectra were measured using an Thermo Scientific NanoDrop 2000 at room temperature (*ca.* 25 °C).

Powder X-ray diffraction (powder-XRD) diagrams were collected on a Panalytical X'pert diffractometer with monochromatic Cu-K α radiation ($\lambda_{\text{Cu}} = 1.5406 \text{ \AA}$). Samples were measured in a capillary.

Nitrogen and carbon dioxide physisorption measurements were performed at 77 K (N₂) and at 298 K (CO₂) using an S4 ASAP 2020 (Micromeritics). Prior to the measurements, the samples were activated by supercritical CO₂ activation. Note here that all synthesized HET-MOPs revealed a loss of crystallinity and an amorphous character after activation (Fig. S14, S22 and S28). The specific surface area (BET) was obtained using the BET equation in the range of 0.001- 0.02 P/P₀ (MicroActive software).

S1.2. Crystallography

Crystallographic data for deprotected Rh₂(bdc)₄ complex, HET-MOP-1, HET-MOP-2 and HET-MOP-3 were collected at 100 K at XALOC beamline at ALBA synchrotron (0.82653 Å).¹ Data were indexed, integrated and scaled using the XDS program.² Absorption correction was not applied. The structures were solved by direct methods and subsequently refined by correction of F² against all reflections, using SHELXT2018 within Olex2 package and WinGX (version 2021.3).^{3,4} All non-hydrogen atoms were refined with anisotropic thermal parameters by full-matrix least-squares calculations on F² using the program SHELXL2018.⁵ We treated the presence of disordered solvent molecules in the cavities of all structures running solvent mask using Olex2 solvent mask or after location of the cage atoms.^{6,7} Besides the 6 DMF molecules and the 3 water molecules (both without coordination to paddle wheels) per formula unit, no additional solvent molecules or sodium ions could be localized in the difference Fourier map of HET-MOP-3 and the SQUEEZE routine of the program PLATON was conversely applied.⁷⁻⁹ Thermal motion of some benzene rings and some coordinated solvents of HET-MOPs were restrained by FLAT, DFIX, DELU, SIMU. For HET-MOP-3 thermal motion of DMF solvent were restrained using EADP. Different Rh/Cu Metal occupancies in the HET-MOPs were tested, including both fixed and freely refined occupancies, as well as by applying EXYZ/EADPs restrains, reaching the most satisfactory refinement indicators for the case where the occupancies are fixed to the 1/3Rh:2/3Cu ratio. Hydrogen atoms were inserted at calculated positions in the three structures. The hydrogen atoms were calculated in their expected positions with the HFIX instruction of SHELXL2018 and refined as riding atoms with Uiso(H) = 1.5 Ueq(C).

(1) Juanhuix, J.; Gil-Ortiz, F.; Cuní, G.; Colldelram, C.; Nicolás, J.; Lidón, J.; Boter, E.; Ruget, C.; Ferrer, S.; Benach, J.; *J. Synchrotron Radiat.* **2014**, *21*, 679-689.

(2) Kabsch, W. *Acta Cryst. D* **2010**, *66*, 125-132.

(3) Sheldrick, G. M. *Acta Cryst. A* **2015**, *71*, 3-8.

(4) Farrugia, L. J. *J. Appl. Cryst.* **2012**, *45*, 849-854.

(5) Sheldrick, G. M. *Acta Cryst. C* **2015**, *71*, 3-8.

(6) Dolomanov, O. V.; Bourhis, L. J.; Gildea, R. J.; Howard, J. A. K.; Puschmann, H. *J. Appl. Cryst.* **2009**, *42*, 339-341.

(7) Spek, A. L. *J. Appl. Cryst.* **2003**, *36*, 7-13.

(8) Spek, A. L. *Acta Cryst.* **2009**, *D65*, 148.

(9) Spek, A. L. *Acta Cryst.* **2015**, *C71*, 9-18.

Table S1. Crystal data and structure refinement for the deprotected Rh₂(bdc)₄ complex.

Identification code	deprotected Rh ₂ (bdc) ₄ complex
CCDC number	2190388
Empirical formula	C ₅₄ H ₇₂ N ₃ O ₁₉ Rh ₂
Formula weight	1272.96
Temperature/K	100
Crystal system	orthorhombic
Space group	Pbcn
a/Å	21.112(2)
b/Å	11.342(3)
c/Å	26.553(3)
α/°	90
β/°	90
γ/°	90
Volume/Å ³	6358(2)
Z	4
ρ _{calc} /cm ³	1.330
μ/mm ⁻¹	0.878
F(000)	2636.0
Crystal size/mm ³	0.24 × 0.07 × 0.07
Radiation	synchrotron (λ = 0.82653)
2θ range for data collection/°	5.066 to 54.666
Index ranges	0 ≤ h ≤ 23, 0 ≤ k ≤ 12, -29 ≤ l ≤ 0
Reflections collected	53152
Independent reflections	4551 [R _{int} = 0.0824, R _{sigma} = 0.0481]
Data/restraints/parameters	4551/1/365
Goodness-of-fit on F ²	1.040
Final R indexes [I ≥ 2σ (I)]	R ₁ = 0.0798, wR ₂ = 0.2229
Final R indexes [all data]	R ₁ = 0.0882, wR ₂ = 0.2449
Largest diff. peak/hole / e Å ⁻³	2.48/-1.09

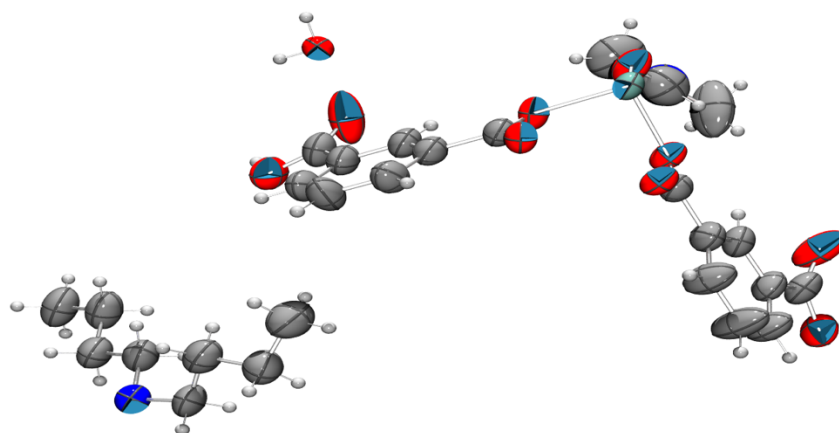


Figure S1. ORTEP diagram of asymmetric unit in the deprotected $\text{Rh}_2(\text{bdc})_4$ complex (50% ellipsoid probability). Color Code: C (grey), N (blue), O (red), H (light grey), and Rh (green).

Table S2. Crystal data and structure refinement for HET-MOP-1.

Identification code	HET-MOP-1
CCDC number	2184149
Empirical formula	$C_{192}H_{112}Cu_{16}O_{120}Rh_8$
Formula weight	6178.73
Temperature/K	100.
Crystal system	tetragonal
Space group	P4/mnc
a/Å	28.7768(6)
b/Å	28.7768(6)
c/Å	27.4035(8)
$\alpha/^\circ$	90
$\beta/^\circ$	90
$\gamma/^\circ$	90
Volume/Å ³	22693
Z	2
$\rho_{\text{calc}}/\text{g}/\text{cm}^3$	0.904
μ/mm^{-1}	1.605
F(000)	6096.0
Crystal size/mm ³	0.09 × 0.06 × 0.06
Radiation	synchrotron ($\lambda = 0.82653$)
2 θ range for data collection/ $^\circ$	2.328 to 49.812
Index ranges	0 ≤ h ≤ 29, 0 ≤ k ≤ 20, 0 ≤ l ≤ 27
Reflections collected	153923
Independent reflections	6469 [$R_{\text{int}} = 0.1088$, $R_{\text{sigma}} = 0.0417$]
Data/restraints/parameters	6469/17/386
Goodness-of-fit on F^2	1.130
Final R indexes [$ I \geq 2\sigma(I)$]	$R_1 = 0.0885$, $wR_2 = 0.2715$
Final R indexes [all data]	$R_1 = 0.1057$, $wR_2 = 0.2980$
Largest diff. peak/hole / e Å ⁻³	1.15/-0.48

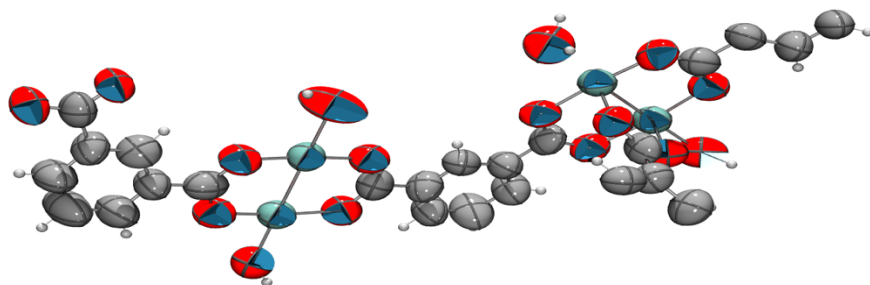


Figure S2. ORTEP diagram of asymmetric unit in the HET-MOP-1 (50% ellipsoid probability). Color Code: C (grey), N (blue), O (red), H (light grey), and Rh (green).

Table S3. Crystal data and structure refinement for HET-MOP-2.

Identification code	HET-MOP-2
CCDC number	2190389
Empirical formula	$C_{213}H_{160}O_{130}N_7Rh_8Cu_{16}$
Formula weight	6732.44
Temperature/K	100
Crystal system	triclinic
Space group	<i>P</i> -1
<i>a</i> /Å	24.910(5)
<i>b</i> /Å	24.930(5)
<i>c</i> /Å	25.120(5)
α /°	98.70(3)
β /°	117.15(3)
γ /°	110.60(3)
Volume/Å ³	12048(6)
Z	1
ρ_{calc} /cm ³	0.928
μ /mm ⁻¹	1.515
F(000)	3349.0
Crystal size/mm ³	0.09 × 0.09 × 0.07
Radiation	synchrotron ($\lambda = 0.82653$)
2 θ range for data collection/°	2.446 to 62.742
Index ranges	-29 ≤ <i>h</i> ≤ 26, -29 ≤ <i>k</i> ≤ 28, 0 ≤ <i>l</i> ≤ 29
Reflections collected	123771
Independent reflections	37536 [$R_{\text{int}} = 0.0928$, $R_{\text{sigma}} = 0.1017$]
Data/restraints/parameters	37536/6/1710
Goodness-of-fit on F ²	1.142
Final R indexes [$I \geq 2\sigma(I)$]	$R_1 = 0.1038$, $wR_2 = 0.3002$
Final R indexes [all data]	$R_1 = 0.1214$, $wR_2 = 0.3217$
Largest diff. peak/hole / e Å ⁻³	2.89/-0.71

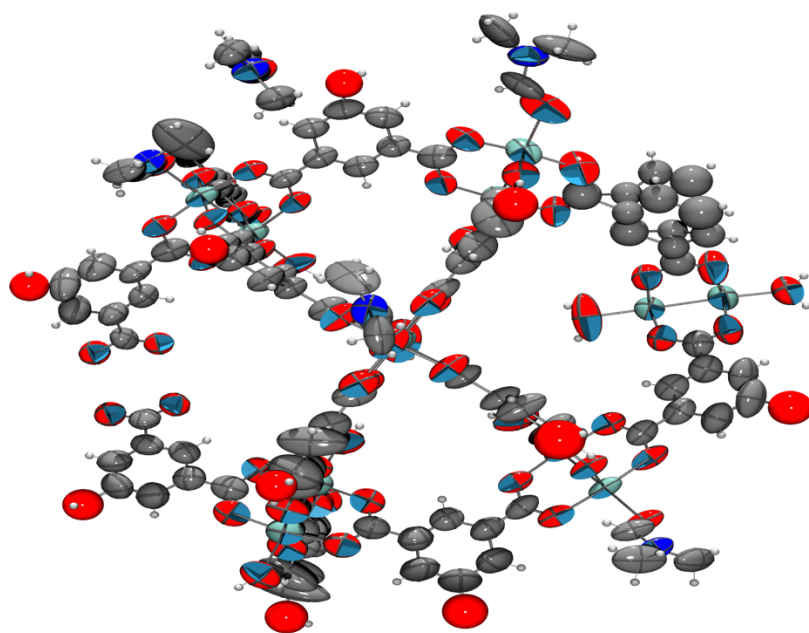


Figure S3. ORTEP diagram of asymmetric unit in the HET-MOP-2 (50% ellipsoid probability). Color code: C (grey), N (blue), O (red), H (light grey), and Rh (green).

Table S4. Crystal data and structure refinement for HET-MOP-3

Identification code	HET-MOP-3
CCDC number	2190390
Empirical formula	$C_{264}H_{280}O_{153}S_8N_{18}Rh_8Cu_{16}$
Formula weight	8249.44
Temperature/K	100
Crystal system	cubic
Space group	<i>Pn-3</i>
<i>a</i> /Å	40.7504(1)
<i>b</i> /Å	40.7504(1)
<i>c</i> /Å	40.7504(1)
α /°	90
β /°	90
γ /°	90
Volume/Å ³	67669.9(5)
Z	4
ρ calc/cm ³	0.810
μ /mm ⁻¹	1.130
F(000)	16664.0
Crystal size/mm ³	0.12 × 0.11 × 0.09
Radiation	synchrotron ($\lambda = 0.82653$)
2 θ range for data collection/°	1.644 to 52.766
Index ranges	0 ≤ <i>h</i> ≤ 25, 1 ≤ <i>k</i> ≤ 43, 0 ≤ <i>l</i> ≤ 43
Reflections collected	559063
Independent reflections	14689 [$R_{int} = 0.1292$, $R_{sigma} = 0.0307$]
Data/restraints/parameters	14689/533/682
Goodness-of-fit on F^2	1.475
Final R indexes [$I \geq 2\sigma(I)$]	$R_1 = 0.1195$, $wR_2 = 0.3418$
Final R indexes [all data]	$R_1 = 0.1350$, $wR_2 = 0.3570$
Largest diff. peak/hole / e Å ⁻³	1.81/-1.05

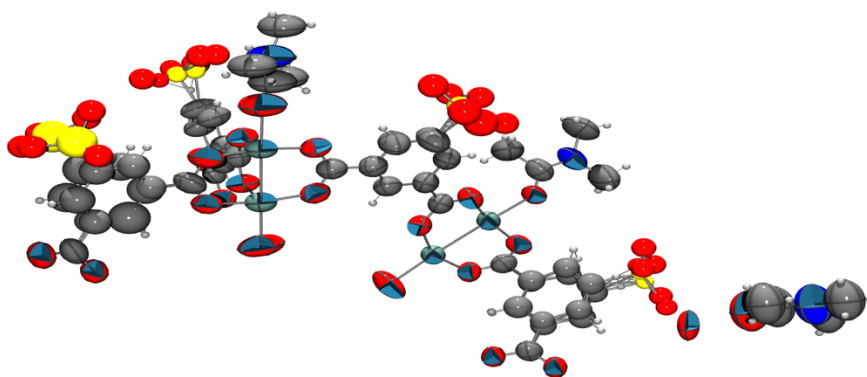
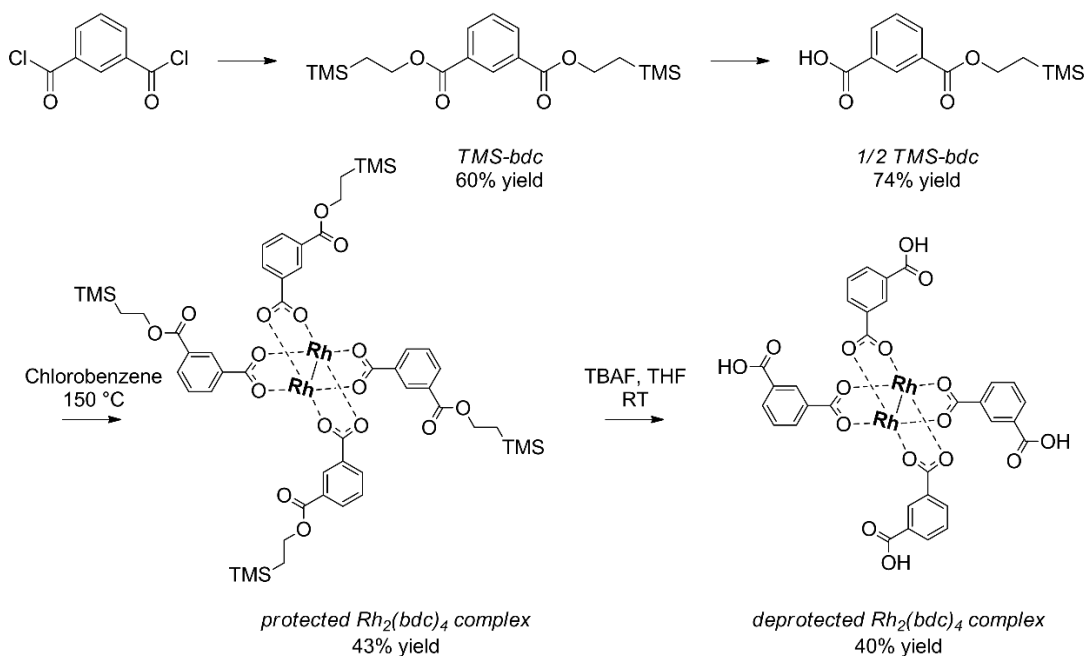


Figure S4. ORTEP diagram of asymmetric unit in the HET-MOP-3 (50% ellipsoid probability). Color code: C (grey), N (blue), O (red), H (light grey), Rh (green), and S (yellow).

S1.3. Synthetic procedures



Scheme S1. Synthesis of $Rh_2(bdc)_4$.

Synthesis of TMS-bdc: Isophthaloyl chloride (1eq., 12 mmol, 2.4 g) was dissolved in 100 mL of DCM using a dry round bottom flask. After stirring for 1 hour, TMS-OH (2.4 eq., 4.1 mL) was added followed by the dropwise addition of 2.8 eq. of pyridine (2.7 mL). After stirring overnight, the mixture was transferred in a separation funnel, washed with 1 M NH_4Cl (3x, 200 mL), 1 M HCl (3x, 200 mL) and water (3x, 250 mL). The organic layer was dried with $MgSO_4$ and concentrated *in vacuo*. Purification by flash chromatography (silica gel, 10% EtOAc in hexanes) yielded the desired product (60% yield) as a transparent oil. **HRMS** (ESI-TOF): m/z calculated for $[NaSi_2O_4C_{18}H_{30}] [M+H]^+$: 389.16; found: 389.16. **1H NMR** (300 MHz, $CDCl_3$): δ = 0.10 (s, 18H, - CH_3); 1.17 (t, J = 8.3 Hz, 4H, - CH_2 -); 4.45 (t, J = 8.3 Hz, 4H, - CH_2 -); 7.52 (t, J = 7.8 Hz, 1H, -CH-); 8.22 (d, J = 7.8 Hz, 2H, -CH-); 8.68 (s, 1H, -CH-) ppm. **^{13}C NMR** (300 MHz, $CDCl_3$): δ = -1.42 (- CH_3); 18.43 (- CH_2 -); 63.63 (- CH_2 -); 128.51 (-CH-); 130.56 (-CH-); 131.06 (-CH-); 133.57 (-CH-); 165.99 (-COO-) ppm.

Synthesis of ½ TMS-bdc: Dry TMS-bdc (1eq., 5 mmol, 1.8 g) was dissolved in 25 mL of THF. After stirring at room temperature for 30 min, a clear solution was obtained. Then, 0.5 eq. of TBAF (1M solution in THF, 2.5 mL) was added followed by stirring at room temperature for 5 hours. Then, another 0.5 eq. of TBAF (1M solution in THF, 2.5 mL) was added to the reaction mixture. After stirring overnight, the obtained solution was poured into ether (100 mL), upon which a white precipitate was obtained. After washing the suspension with 0.5 M HCl (3x 100 mL) and water (3x 100 mL), the clear organic phase was dried with MgSO₄ and concentrated *in vacuo*. The product was obtained in 74% yield as a white solid. **HRMS** (ESI-TOF): m/z calculated for [SiO₄C₁₃H₁₇] [M-H]⁻: 265.09; found: 265.09. **¹H NMR** (300 MHz, DMSO-d₆): δ = 0.06 (s, 9H, -CH₃); 1.11 (t, *J* = 8.3 Hz, 2H, -CH₂-); 4.40 (t, *J* = 8.3 Hz, 2H, -CH₂-); 7.66 (m, *J* = 7.4 Hz, 1H, -CH-); 8.17 (t, *J* = 7.4 Hz, 2H, -CH-); 8.49 (s, 1H, -CH-) ppm. **¹³C NMR** (300 MHz, DMSO-d₆): δ = -0.98 (-CH₃); 17.29 (-CH₂-); 63.61 (-CH₂-); 129.74 (-CH-); 130.16 (-CH-); 130.89 (-CH-); 131.81 (-CH-); 133.56 (-CH-); 134.12 (-CH-); 165.52 (-COO-); 166.92 (-COOH) ppm.

Synthesis of the protected Rh₂(bdc)₄ complex. Rhodium acetate (1 eq.; 0.15 mmol, 66.3 mg) and ½TMS-bdc (4 eq.; 0.6 mmol, 138.2 mg) were suspended in 20 mL of chlorobenzene. The mixture was stirred under reflux overnight. Then, the solvent was evaporated and the crude product was redissolved in dichloromethane (40 mL). Reduced rhodium (0) was removed by centrifugation, and the green solution was again dried *in vacuo*. Purification by flash chromatography (silica gel, 2-10% EtOAc in DCM) yielded the desired product (43% yield). **HRMS** (MALDI): m/z calculated for [Rh₂Si₄O₁₆C₅₂H₆₈] [M-H]⁻: 1266.1; found: 1267.9. **¹H NMR** (300 MHz, CDCl₃): δ = 0.06 (s, 9H, -CH₃); 1.14 (t, *J* = 8.3 Hz, 2H, -CH₂-); 4.40 (t, *J* = 8.3 Hz, 2H, -CH₂-); 7.36 (t, *J* = 7.8 Hz, 1H, -CH-); 8.07 (d, *J* = 7.8 Hz, 1H, -CH-); 8.16 (d, *J* = 7.8 Hz, 1H, -CH-); 8.62 (s, 1H, -CH-) ppm. **¹³C NMR** (300 MHz, CDCl₃): δ = 1.11 (-CH₃); 17.52 (-CH₂-); 63.55 (-CH₂-); 127.78 (-CH-); 130.19 (-CH-); 130.34 (-CH-); 131.50 (-CH-); 132.95 (-CH-); 133.17 (-CH-); 166.15 (-COO-); 184.3 (-COORh-) ppm.

Synthesis of the deprotected Rh₂(bdc)₄ complex. The protected Rh₂(bdc)₄ complex (0.1 mmol, 126.8 mg) was dissolved in 10 mL of THF followed by the addition of 4.8 eq. of TBAF (1M solution in THF, 0.48 mL). After stirring at room temperature overnight, the suspension was centrifuged. The obtained green solid was washed with THF (3x 40 mL) and ether (3x 40 mL) and left under open air to dry (40% yield). Single crystals were obtained by slow evaporation of a solution of the deprotected Rh₂(bdc)₄ complex in a water acetone mixture. **HRMS** (MALDI): m/z calculated for

[Rh₂O₁₆C₃₂H₂₀] [M]: 866.3; found: 865.9. ¹H NMR (300 MHz, DMSO-d₆): δ = 7.30 (t, *J* = 7.8 Hz, 1H, -CH-); 7.82 (d, *J* = 7.8 Hz, 1H, -CH-); 7.91 (d, *J* = 7.8 Hz, 1H, -CH-); 8.28 (s, 1H, -CH-) ppm.

Synthesis of HET-MOP-1:

The deprotected Rh₂(bdc)₄ complex (1 eq., 0.012 mmol, 10.4 mg) was dissolved in 0.1 mL of DMA followed by the addition of a solution of bdc (2 eq., 0.024 mmol, 4.0 mg) in 0.1 mL of DMA. Then, Cu(NO₃)₂·3H₂O (4 eq., 0.048 mmol, 11.6 mg) in 0.1 mL of DMA was added. The obtained solution was kept at room temperature for 1 week. After centrifugation, a green solid (13% yield) was obtained, which was washed with DMA (3x 0.5 mL) and Et₂O (3x 1 mL). The wet solid was redissolved in DMF and, upon addition of 4-*tert*-butylpyridine and exposure to ether vapours, single crystals were obtained.

Synthesis of HET-MOP-2:

The deprotected Rh₂(bdc)₄ complex (1 eq., 0.012 mmol, 10.4 mg) was dissolved in 0.1 mL of DMA followed by the addition of a solution of OH-bdc (2 eq., 0.024 mmol, 4.4 mg) in 0.1 mL of DMA. Then, Cu(NO₃)₂·3H₂O (4 eq., 0.048 mmol, 11.6 mg) in 0.1 mL of DMA was added. The obtained solution was kept at room temperature for 1 week. After centrifugation, a green solid (14% yield) was obtained, which was washed with DMA (3x 0.5 mL) and Et₂O (3x 1 mL). The wet solid was redissolved in DMF and single crystals were obtained upon exposure to ether vapours.

Synthesis of HET-MOP-3:

The deprotected Rh₂(bdc)₄ complex (1 eq., 0.012 mmol, 10.4 mg) was dissolved in 0.1 mL of DMA followed by the addition of a solution of NaSO₃-bdc (2 eq., 0.024 mmol, 6.4 mg) in 0.1 mL of DMA. Then, Cu(NO₃)₂·3H₂O (4 eq., 0.048 mmol, 11.6 mg) in 0.1 mL of DMA was added. The obtained solution was kept at 85 °C for 48 hours, yielding green crystals suitable for single-crystal X-ray diffraction (25% yield). The obtained crystals were carefully washed with DMA (3x 0.1 mL) and Et₂O (1x 1 mL).

Acid digestions of Rh₂(bdc)₄ complexes and MOPs at high temperature:

In a typical experiment, 2-5 mg of each HET-MOP were dispersed in 400 μL DMSO-d₆, followed by the addition of 20 μL of deuterium chloride (DCI, 20wt% in D₂O). The yellow mixture was kept at 100 °C for 1 hour and further analysed through ¹H NMR.

Acid digestion of MOPs at room temperature to elucidate the deprotected $\text{Rh}_2(\text{bdc})_4$ complex to linker ratio:

In a typical experiment, 2-5 mg of each HET-MOP were dispersed in 400 μL DMSO-d_6 , followed by the addition of 20 μL of deuterium chloride (DCI, 2wt% in $\text{D}_2\text{O}/\text{DMSO-d}_6$). The orange mixture was directly analysed through ^1H NMR.

S2. Characterization of organic linkers

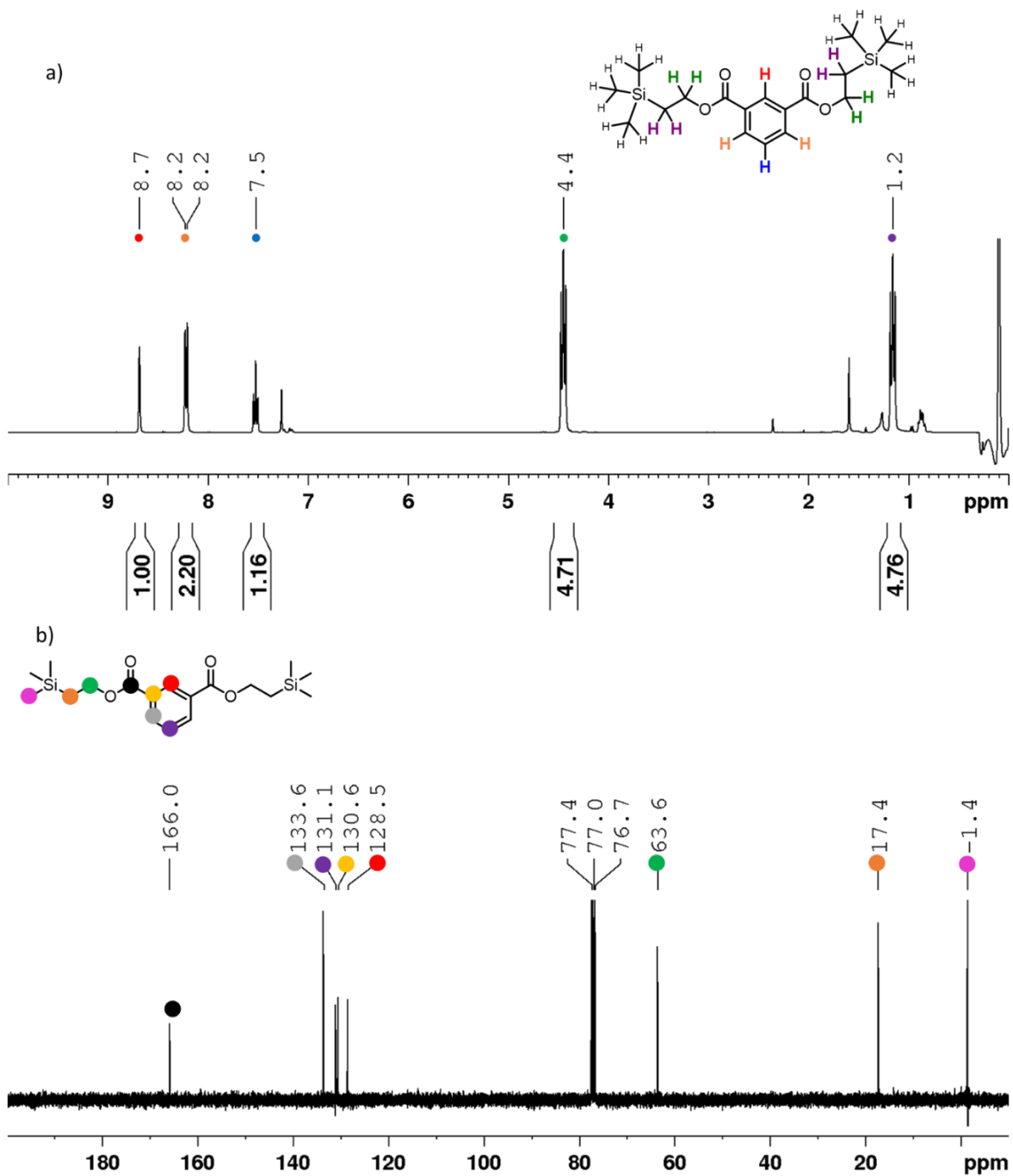


Figure S5. A) ^1H NMR (300 MHz, CDCl_3) spectrum of TMS-bdc. B) ^{13}C NMR (300 MHz, CDCl_3) spectrum of TMS-bdc.

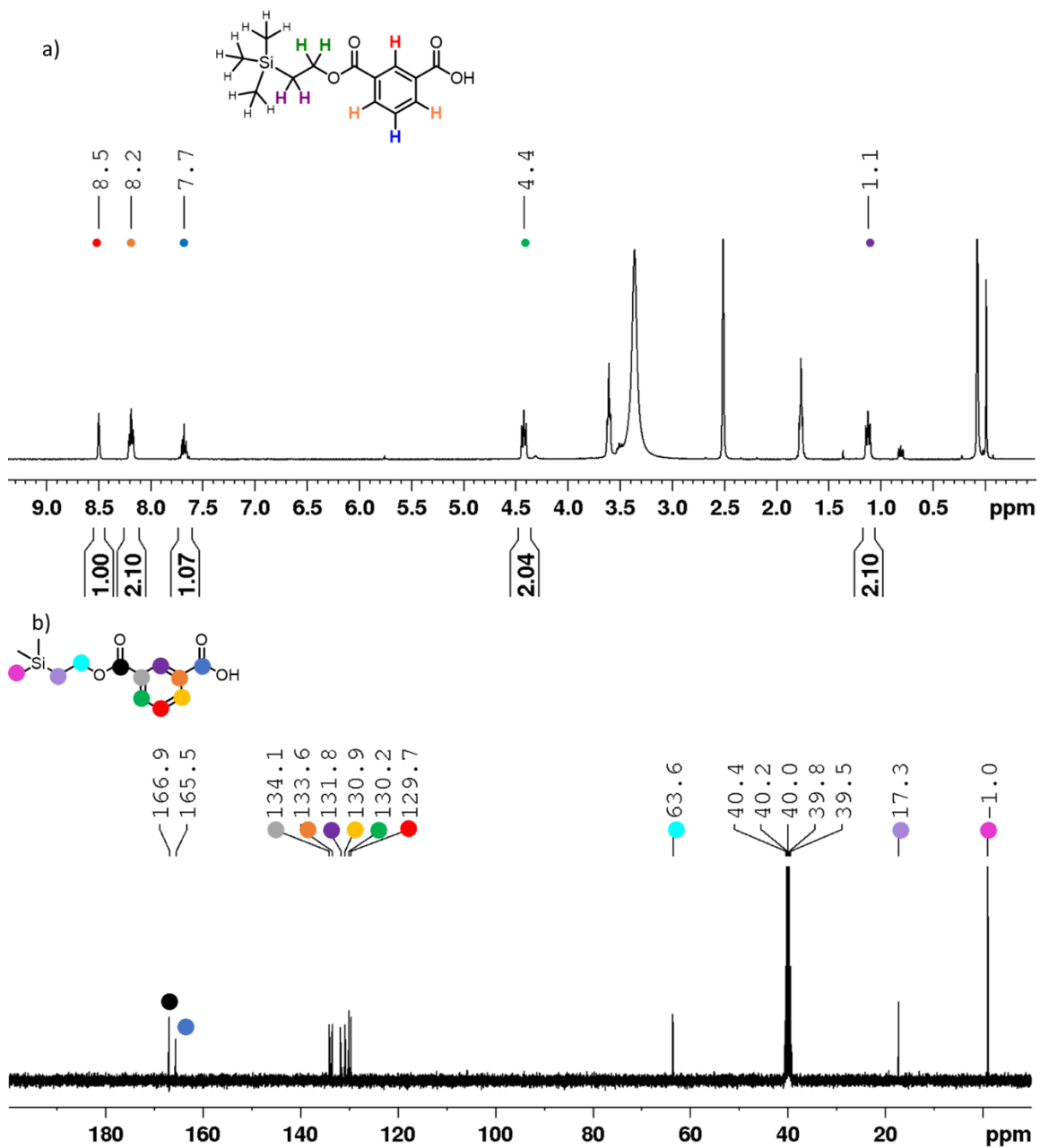
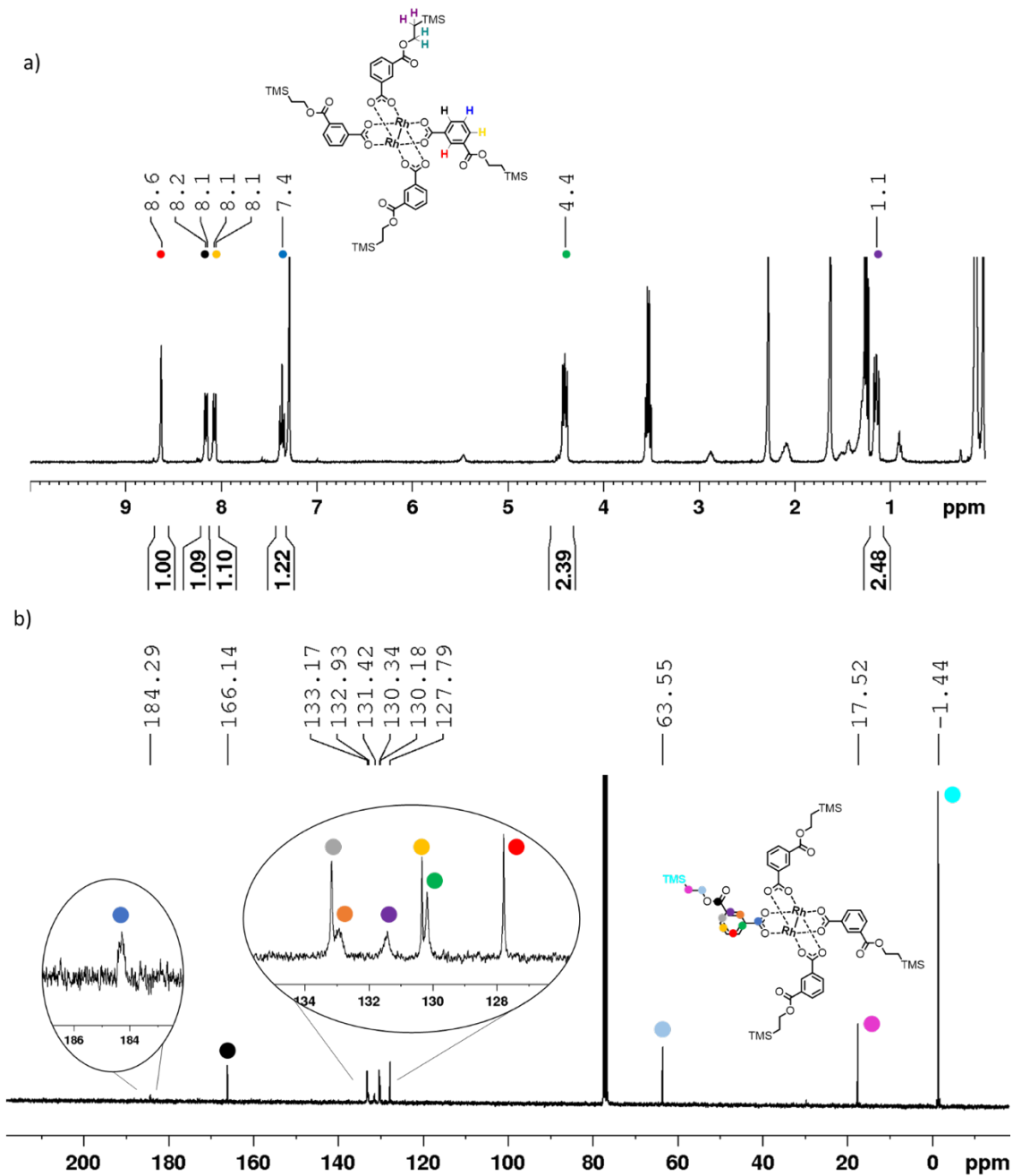


Figure S6. a) ^1H NMR (300 MHz, DMSO-d_6) spectrum of $\frac{1}{2}$ TMS-bdc. b) ^{13}C NMR (300 MHz, DMSO-d_6) spectrum of $\frac{1}{2}$ TMS-bdc.

S3. Characterization of Rh(II)-based metal-organic complexes.



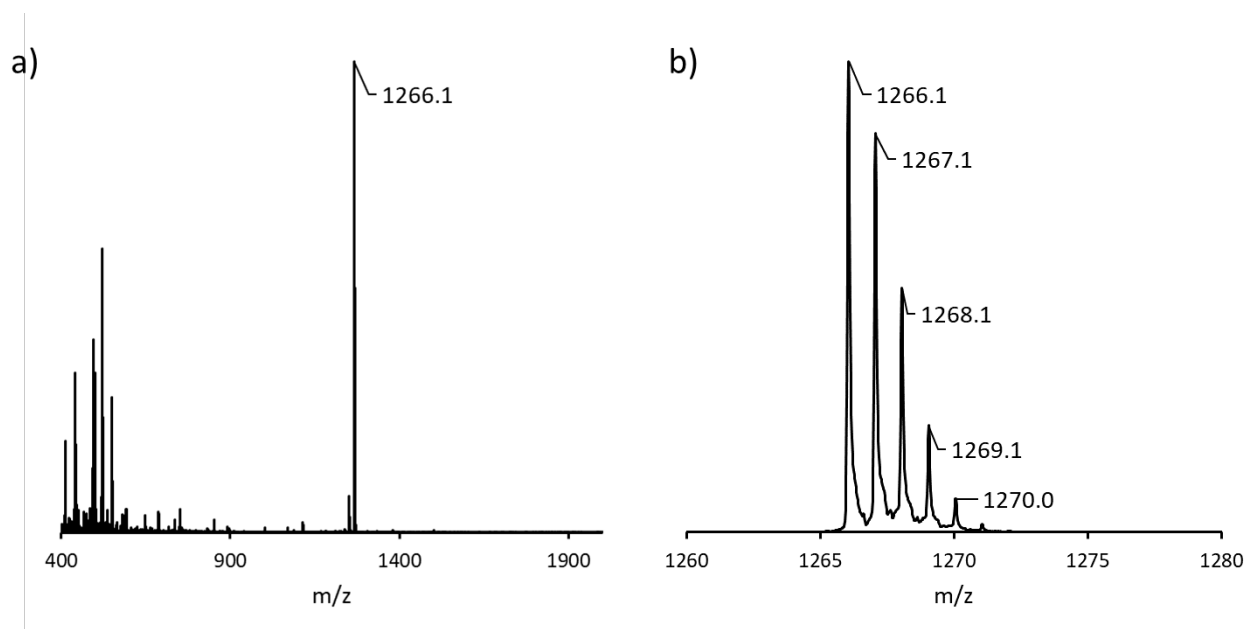


Figure S8. a) MALDI-TOF spectrum for the protected $\text{Rh}_2(\text{bdc})_4$ complex. b) Higher magnification of the relevant m/z region. m/z calculated for $[\text{Rh}_2\text{Si}_4\text{O}_{16}\text{C}_{52}\text{H}_{68}] [\text{M}-\text{H}]^-$: 1266.1.

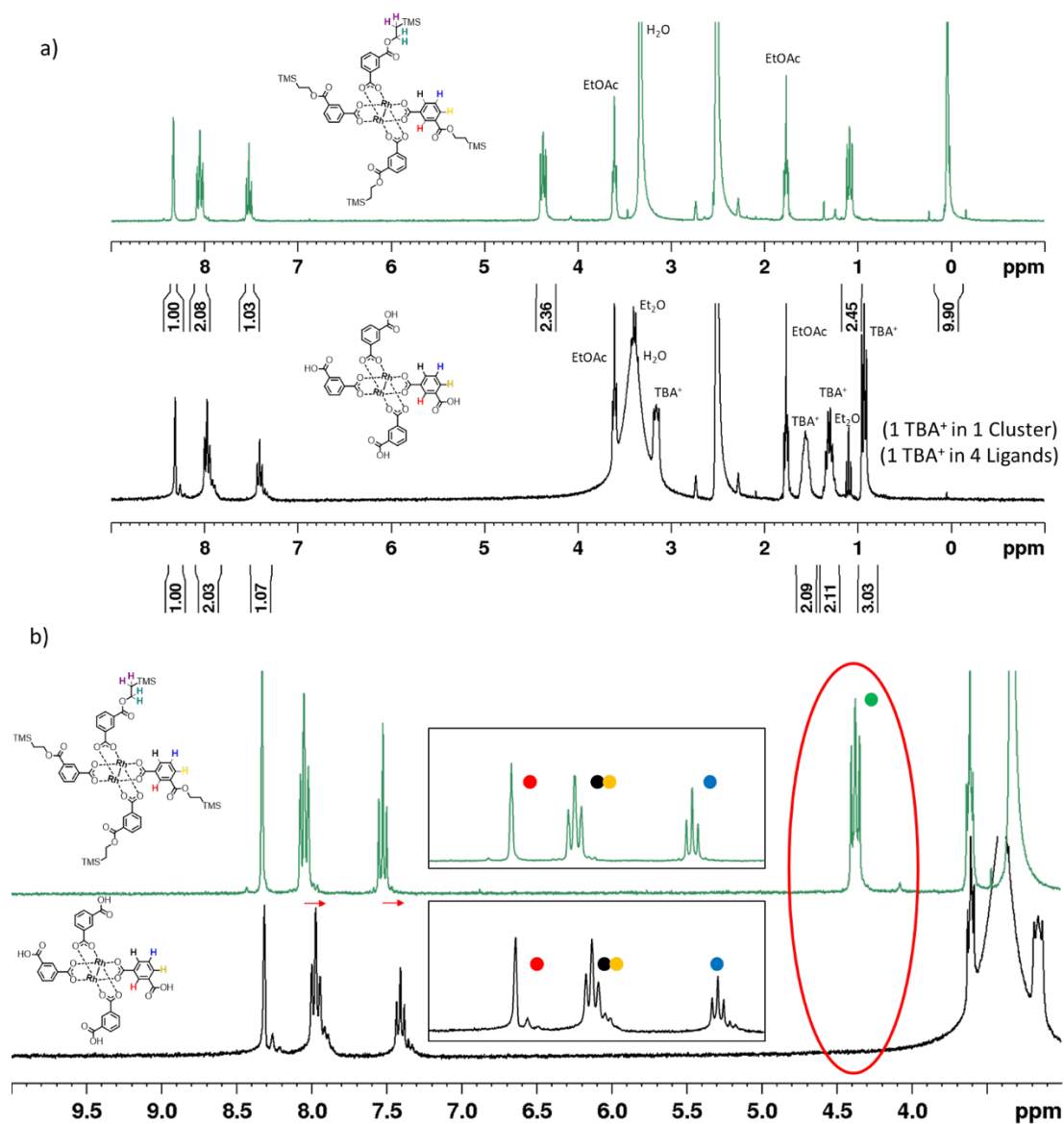


Figure S9. a) ^1H NMR spectra (300 MHz, DMSO-d_6) of the deprotected (black) and protected (green) $\text{Rh}_2(\text{bdc})_4$ complex. b) Zoom-in of the aromatic region, in which the disappearance of the protecting group has been highlighted in red. Please note that, depending on the amount of remaining TBA $^+$ and the orientation of the ligand in the cluster, the signals in the aromatic region can be duplicated and broadened (two singlets, two triplets and two triplets).

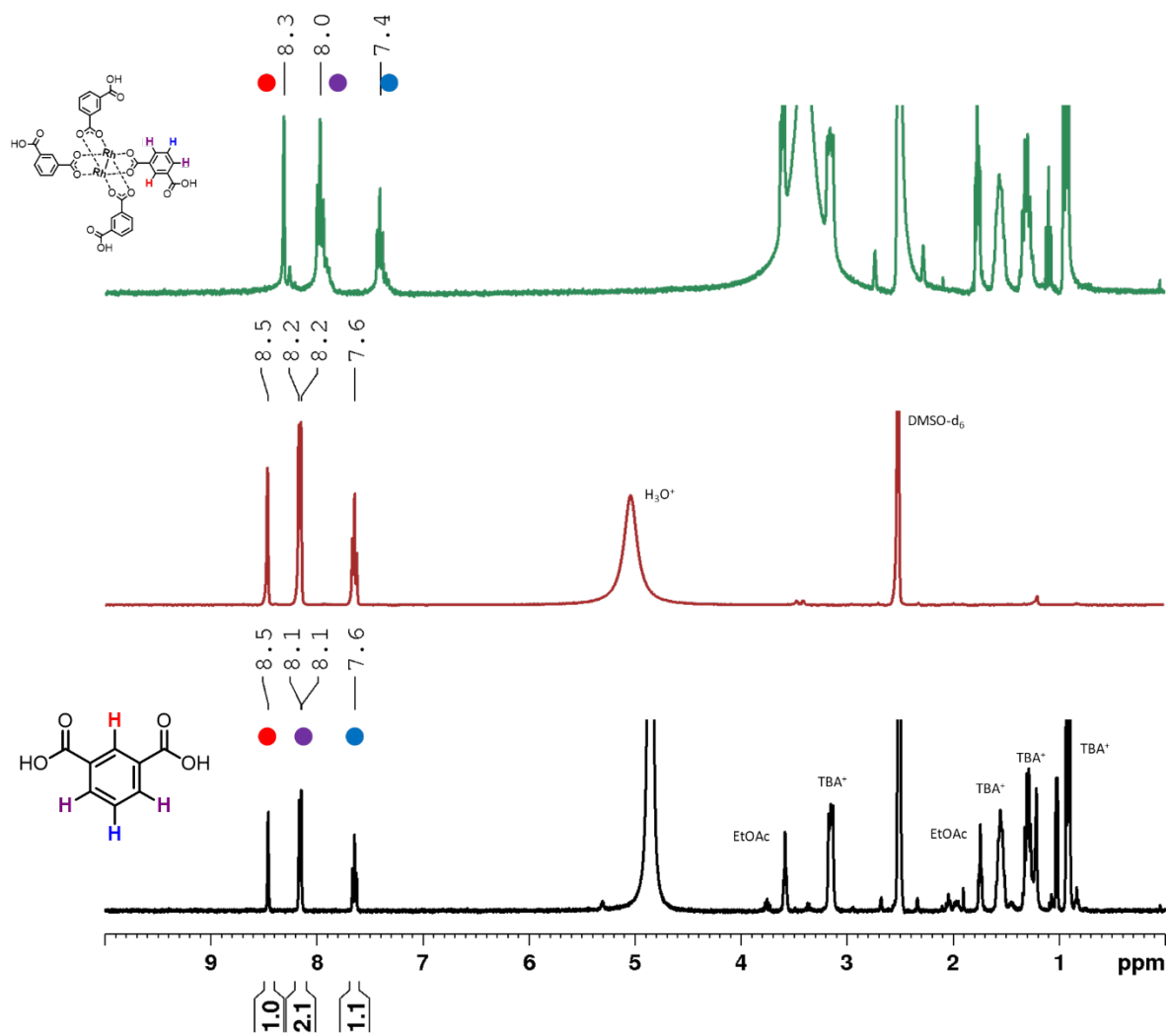


Figure S10. ^1H NMR spectra (300 MHz, DMSO-d_6) of the solution containing the deprotected $\text{Rh}_2(\text{bdc})_4$ complex obtained before (green) and after (black) digesting under acidic conditions at high temperature ($T = 100\text{ }^\circ\text{C}$). In red, the ^1H NMR spectrum of bdc under similar digesting conditions.

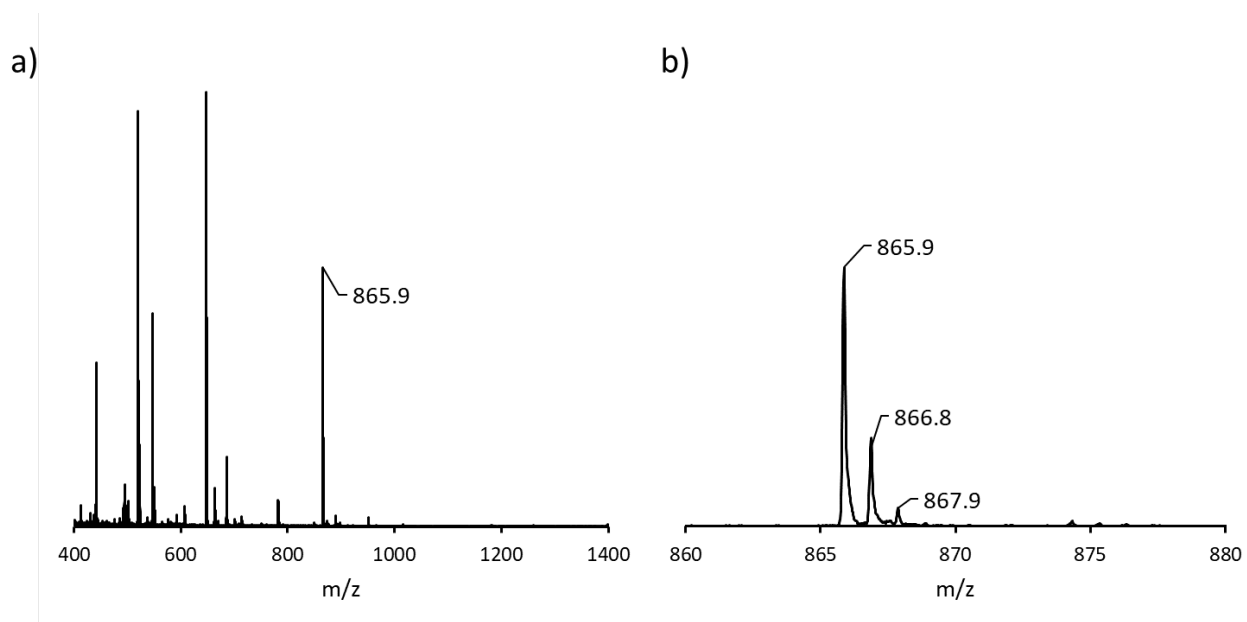


Figure S11. a) MALDI-TOF spectrum for the deprotected $\text{Rh}_2(\text{bdc})_4$ complex. b) Higher magnification of the relevant m/z region. m/z calculated for $[\text{Rh}_2\text{O}_{16}\text{C}_{32}\text{H}_{20}] [\text{M}]$: 865.9.

S4. Characterization of HET-MOP-1

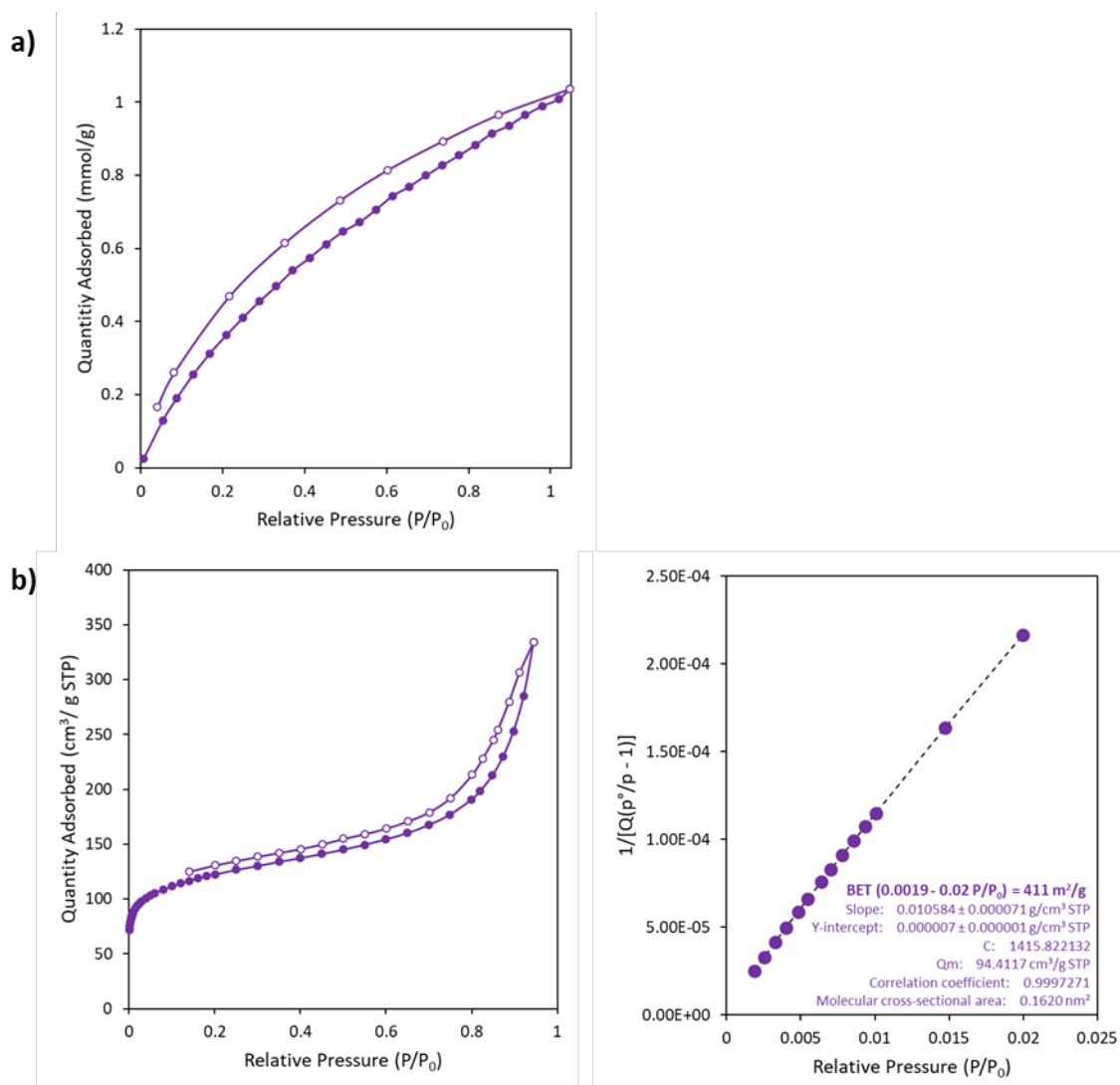


Figure S12. Gas adsorption isotherms for a) CO₂ at 298 K and b) N₂ at 77 K of HET-MOP-1. Solid line depicts adsorption and dashed line shows desorption.

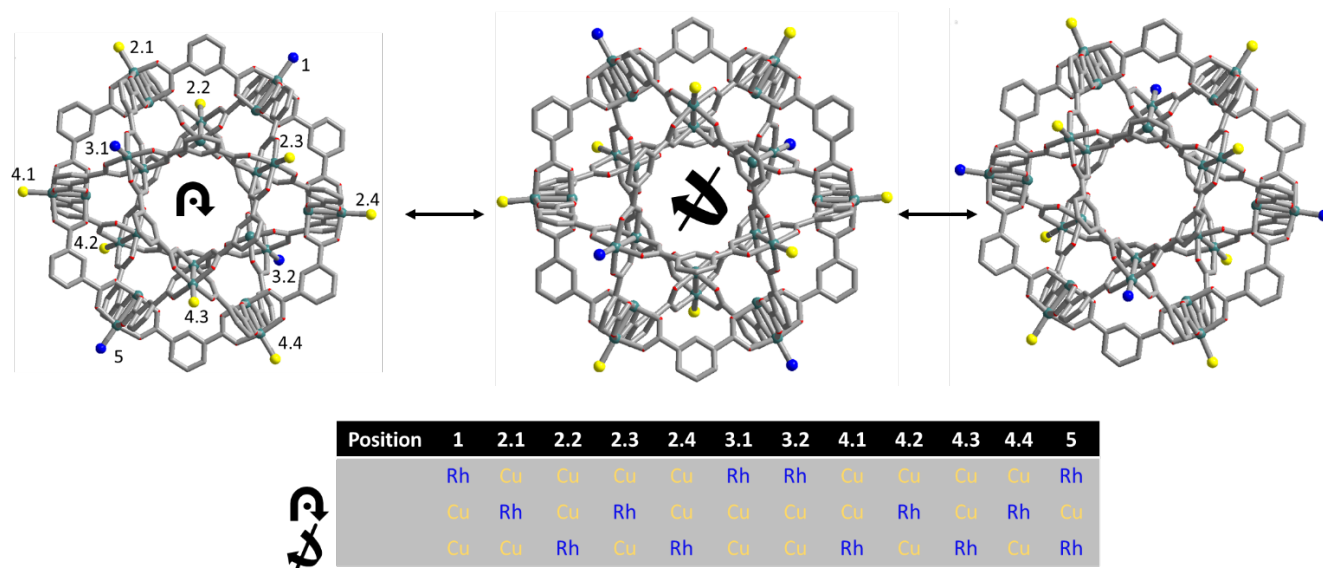


Figure S13. Schematic showing the relationship between the symmetry of the cuboctahedra MOP and the occupancy of each metal center in each crystallographic position. Each metal site has been labelled as shown in the left side of the scheme. Rh(II) sites are highlighted by placing a blue sphere on their axial site, whereas the Cu(II) sites are indicated by a yellow sphere. It can be observed how the rotation of the MOP leads to isomeric MOP structures in which the nature of each metal center is changed. The average of all these isomeric structures indicates that each metal center is occupied 1/3 of the times by Rh(II) ions and 2/3 of the times by Cu(II) ions.

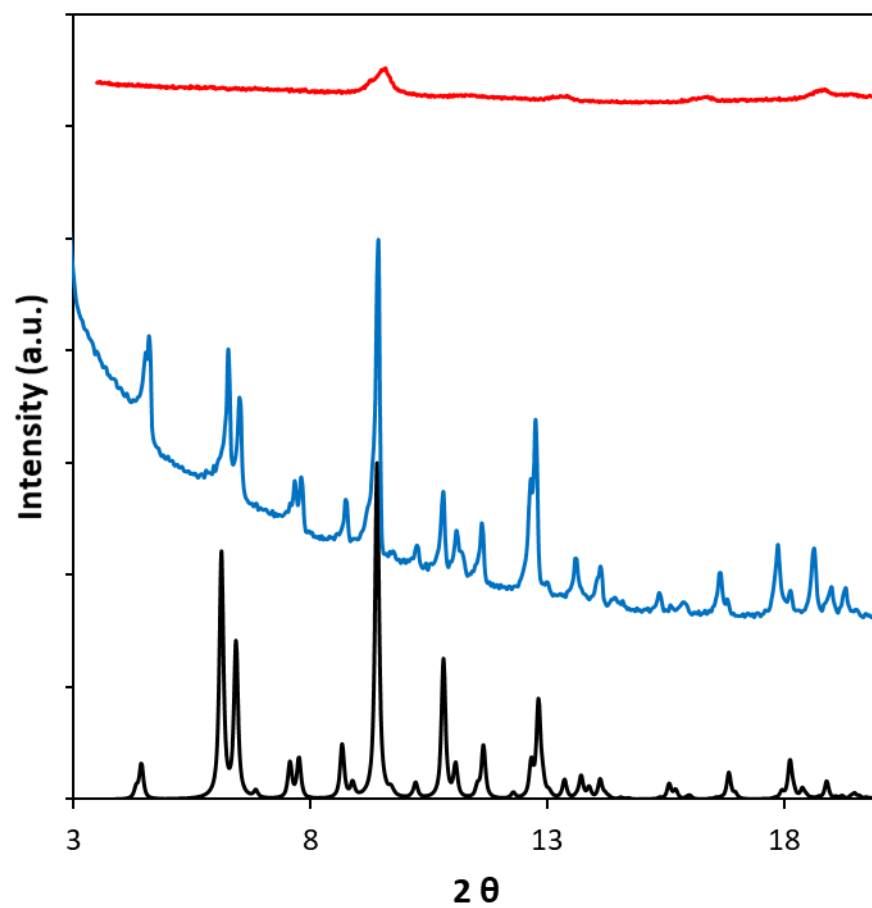


Figure S14. Simulated (black) and experimental (blue) powder-XRD diffractograms of HET-MOP-1. In red, PXRD of activated HET-MOP-1 for the adsorption measurements.

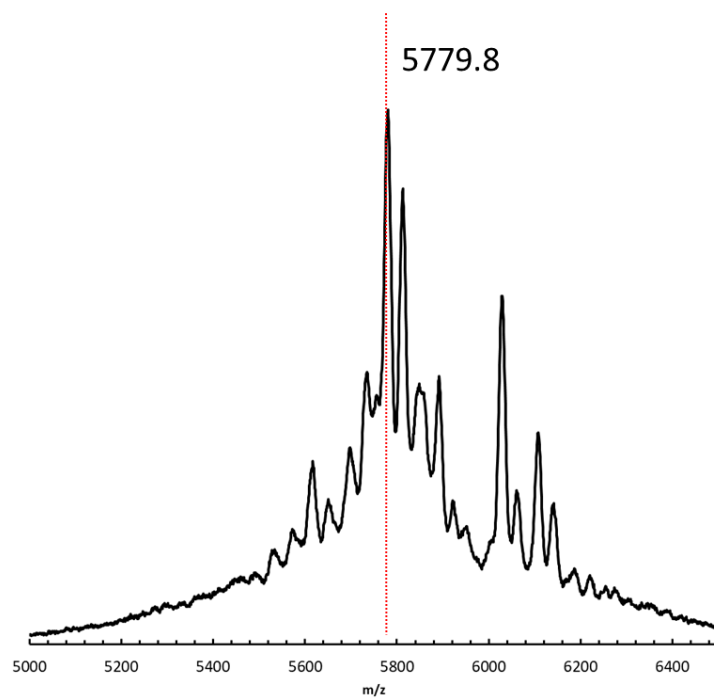


Figure S15. MALDI-TOF spectrum of HET-MOP-1-. Expected molecular mass ($[M+H]^+$) = 5779.4.

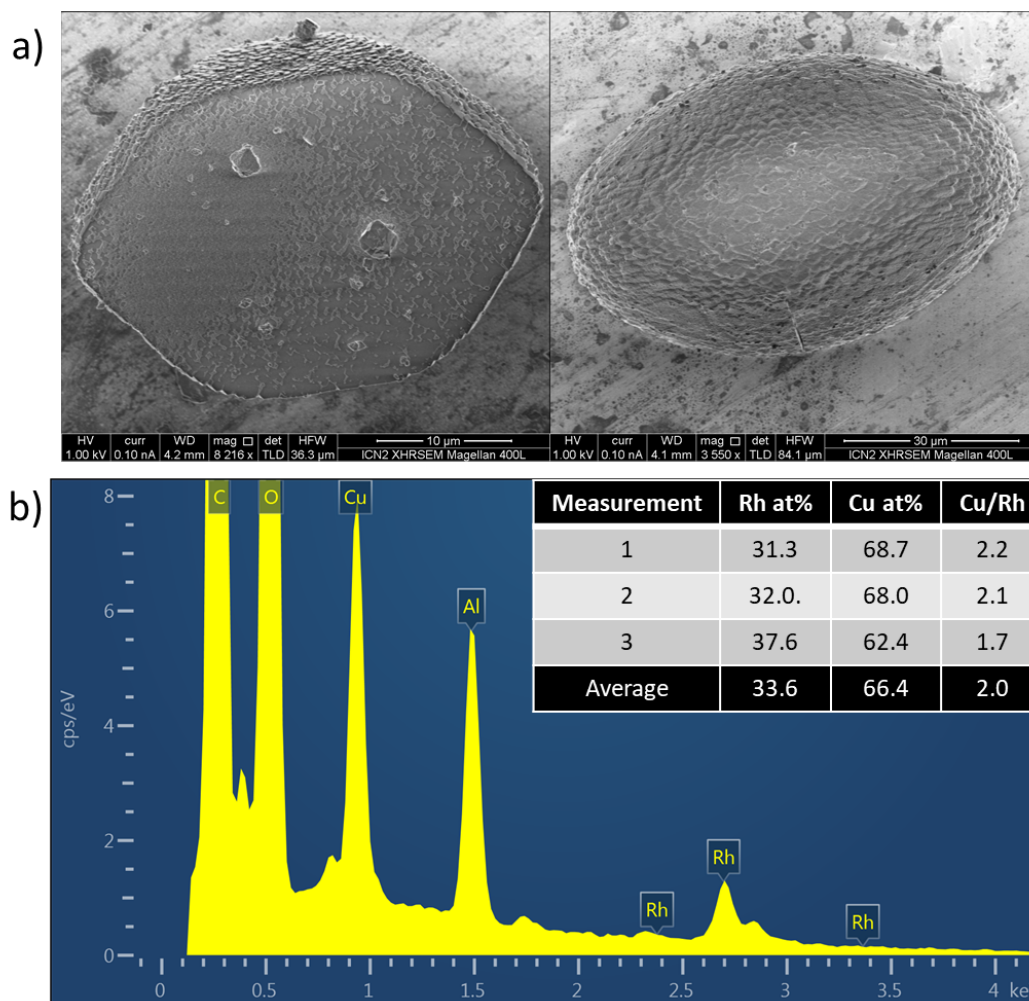


Figure S16. a) High resolution SEM images of two single crystal of HET-MOP-1. b) Corresponding EDX data of a single crystal of HET-MOP-1 with the inset showing the atomic percentage of Rh(II) and Cu(II) ions.

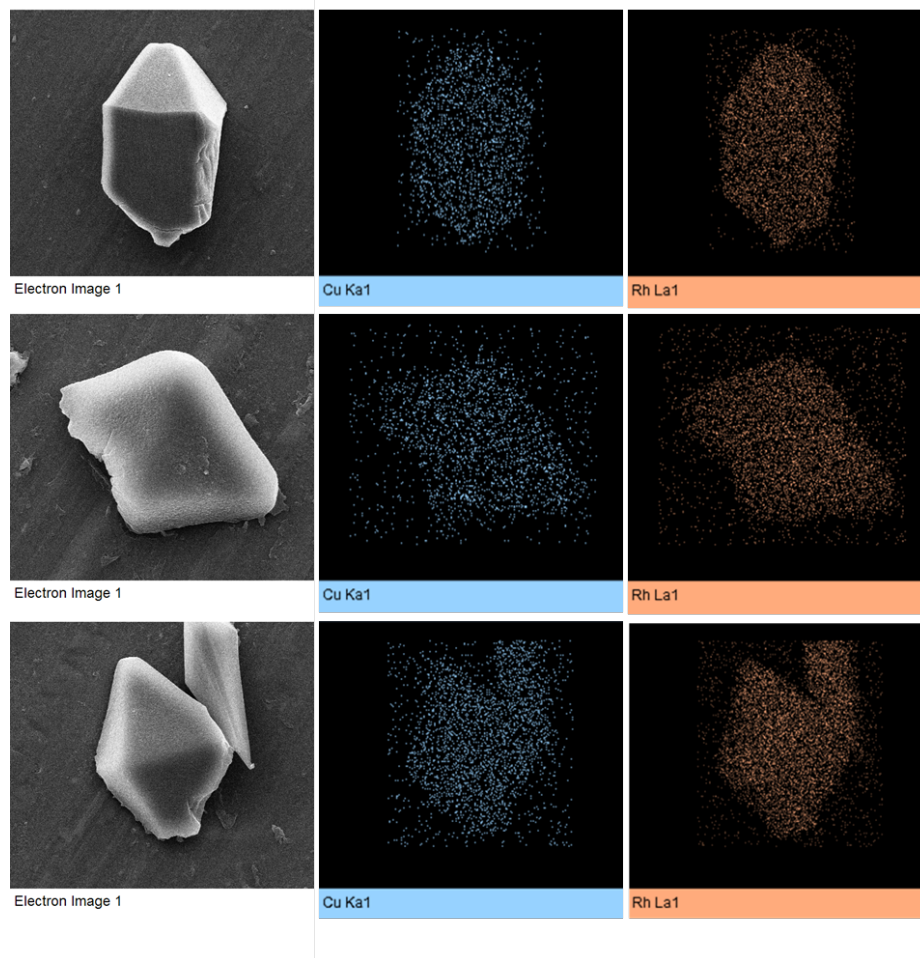


Figure S17. EDX Mapping of three different single crystals of HET-MOP-1.

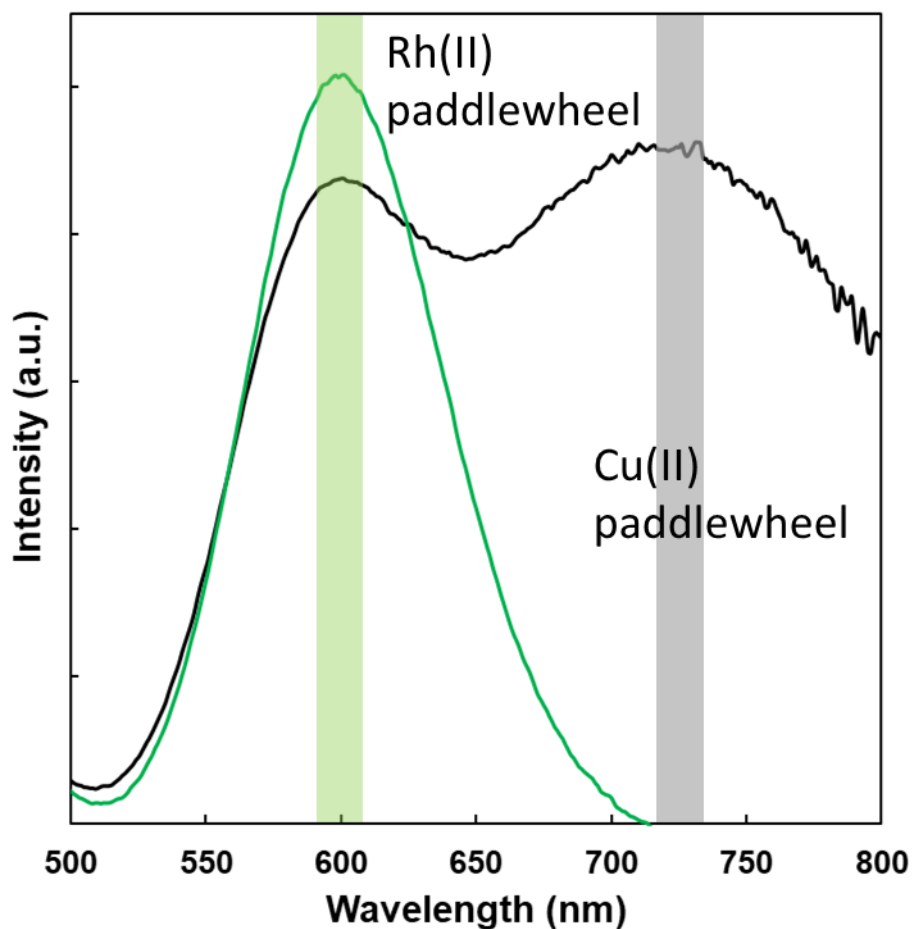


Figure S18. UV/Vis spectrum of HET-MOP-1 (black) showing the presence of both Rh(II) and Cu(II) paddlewheels. For comparison purposes, it is shown the UV/Vis spectrum of the deprotected $\text{Rh}_2(\text{bdc})_4$ complex (green). Note here that these spectra indicate that the structure of HET-MOP-1 contains homogenous Rh(II) and Cu(II) paddlewheels, excluding the presence of mixed metal paddlewheels.

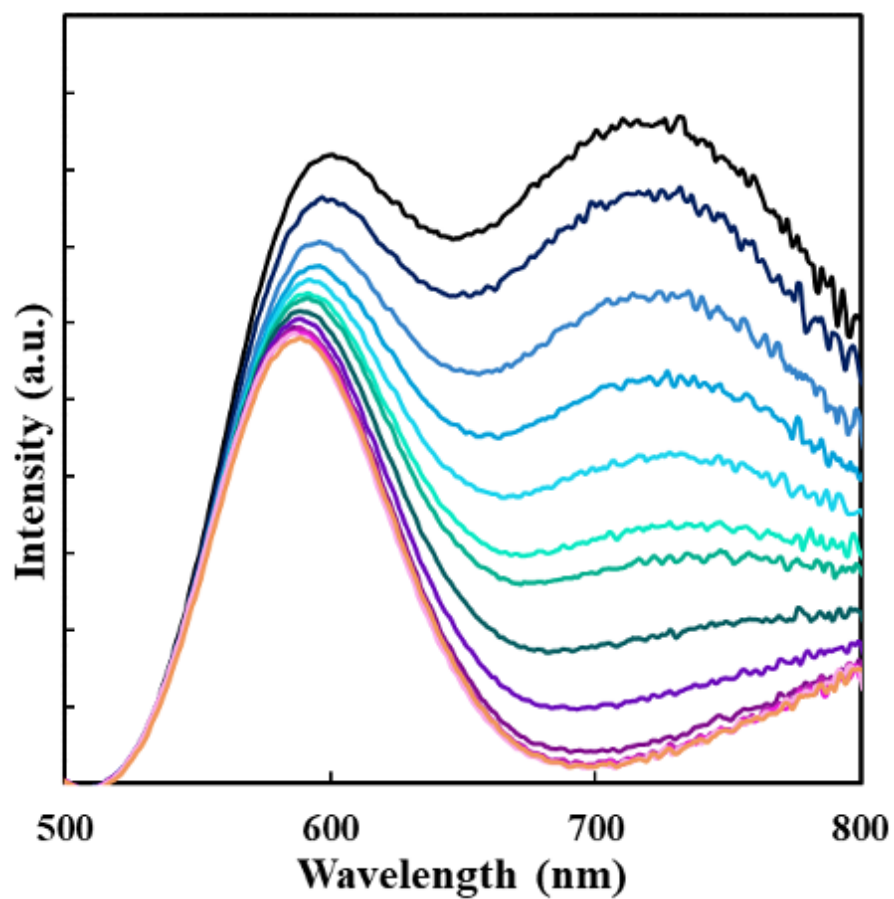


Figure S19. UV-Vis spectra obtained during titration of HET-MOP-1 with HCl (0.1 M), from 1 eq. (top) to 12 eq. (bottom). The red spectrum corresponds to reaction of HET-MOP-1 with 12 eq. HCl for 1 hour.

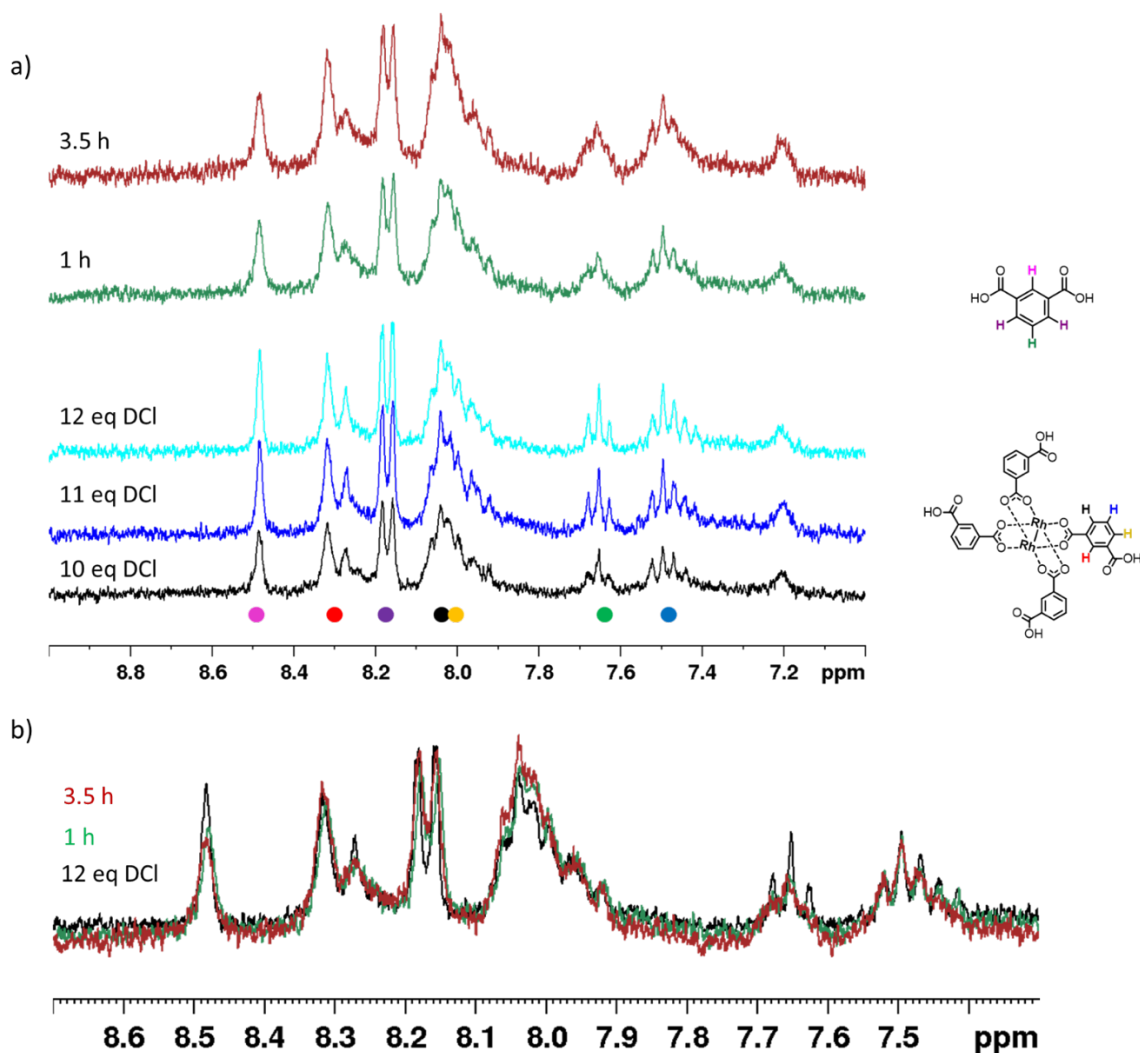


Figure S20. a) ^1H NMR spectra (300 MHz, DMSO-d_6) of the stepwise disassembly of HET-MOP-1 at room temperature using up to 12 mol. eq. of DCl. b) Overlap of the spectra obtained immediately after the addition of 12 mol. eq. of DCl to HET-MOP-1 (black), after 1 hour (green) and after 3.5 hours (red). These results show that the deprotected $\text{Rh}_2(\text{bdc})_4$ complex is stable even after being stored for 3.5 hours in the acidic solution, which enables to elucidate the complex to bdc linker molar ratio.

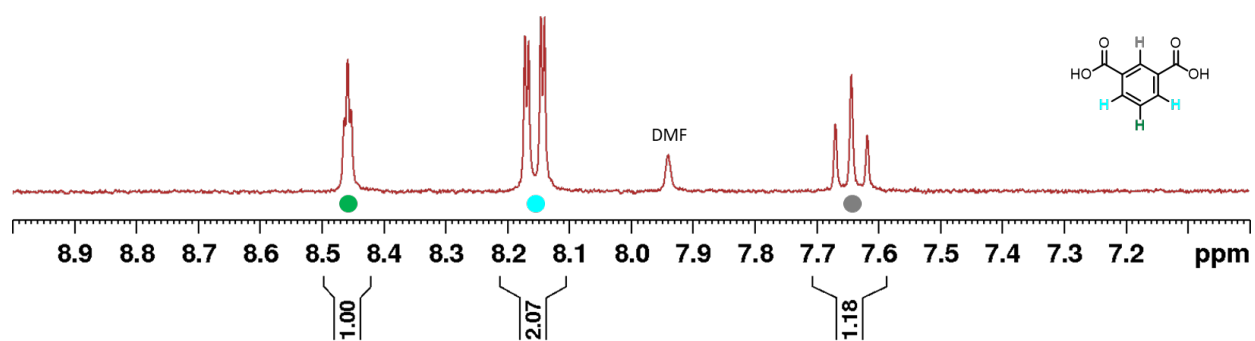


Figure S21. ^1H NMR (300 MHz, DMSO-d_6) spectrum of the acidic disassembly at $100\text{ }^\circ\text{C}$ of HET-MOP-1, showing the degradation of the deprotected $\text{Rh}_2(\text{bdc})_4$ complex at high temperature and the appearance of the signals ascribed to free bdc.

S5. Characterization of HET-MOP-2

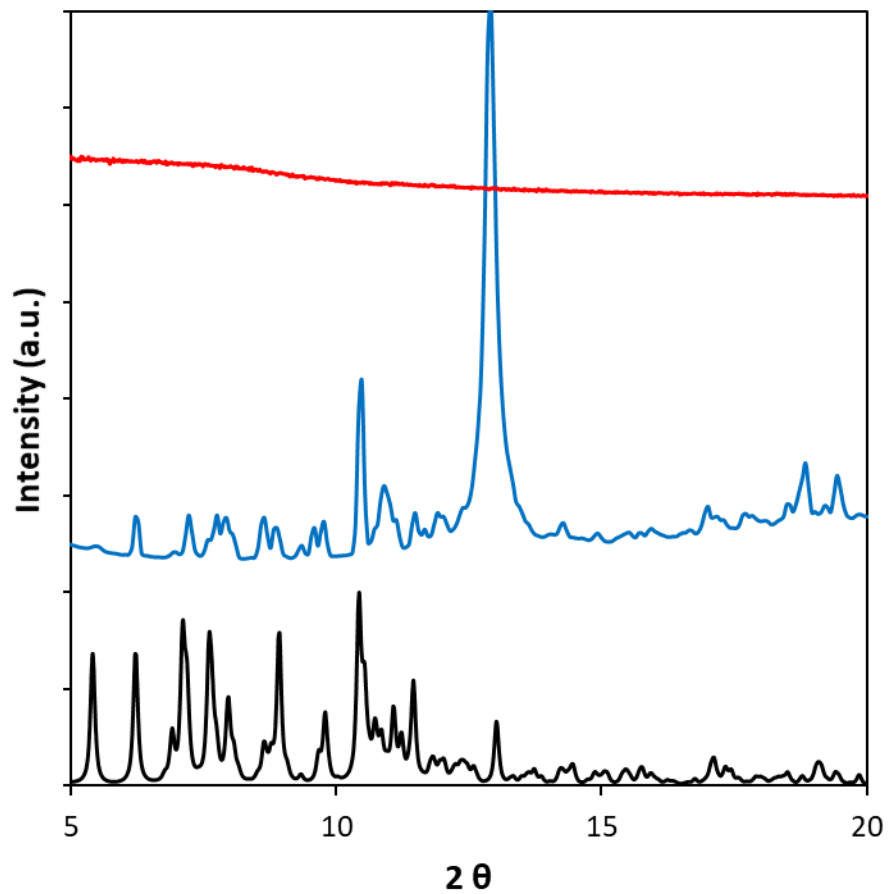


Figure S22. Simulated (black) and experimental (blue) powder-XRD diffractograms of HET-MOP-2. In red, PXRD of activated HET-MOP-2 for the adsorption measurements.

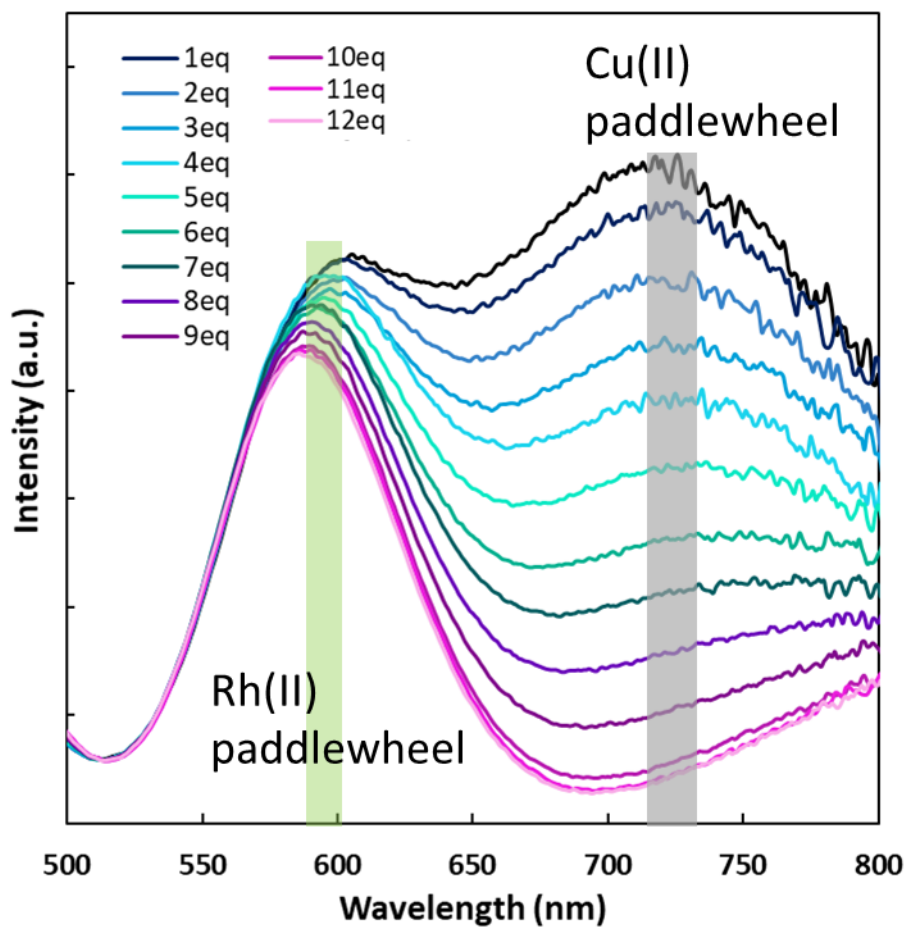


Figure S23. UV/Vis spectra of the disassembly of HET-MOP-2 with increasing amount of HCl (0.1 M) from 1 eq. to 12 eq. at room temperature.

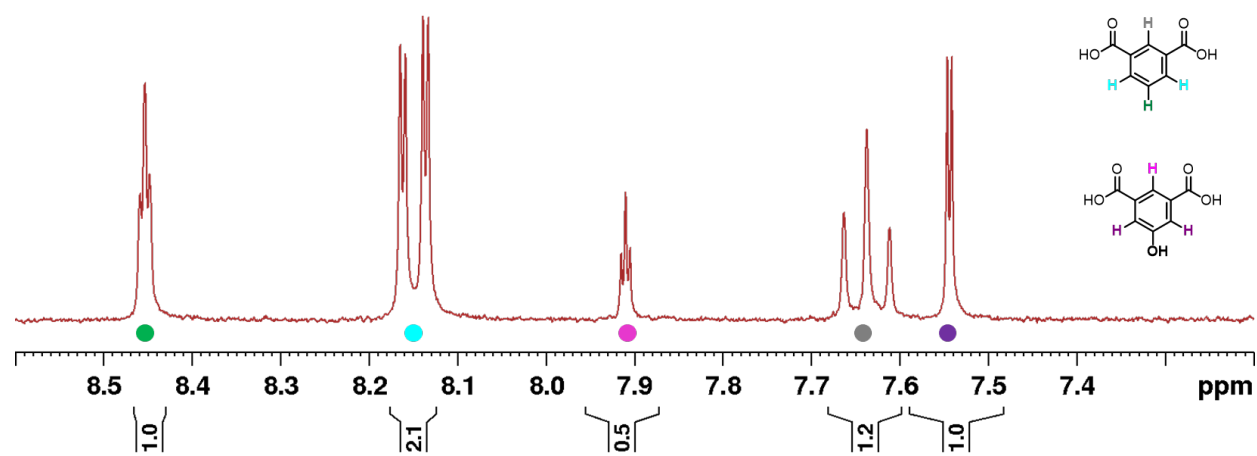


Figure S24. ^1H NMR spectrum (300 MHz, DMSO-d_6) of the acidic disassembly at 100 °C of HET-MOP-2, showing the appearance of the signals ascribed to free OH-bdc and bdc.

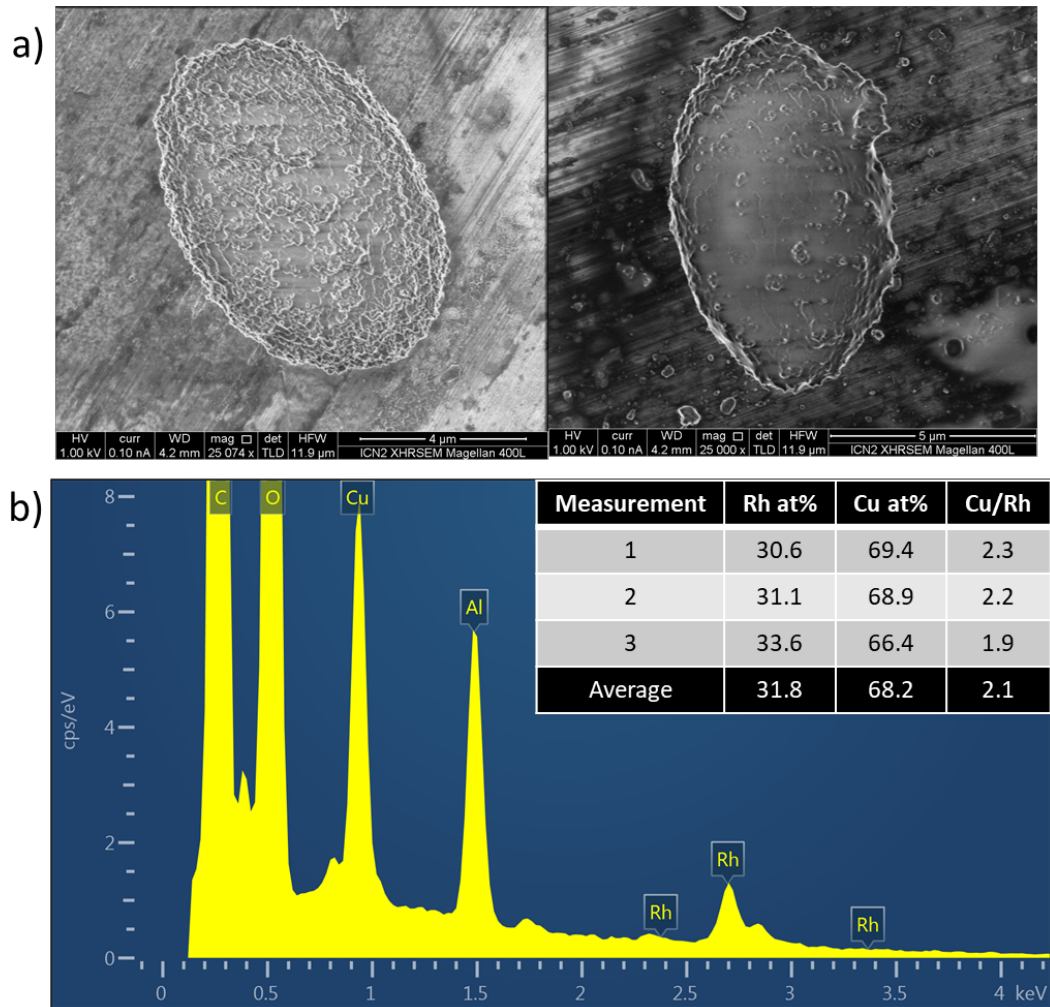


Figure S25. a) High resolution SEM images of two single crystal of HET-MOP-2. b) Corresponding EDX data of a single crystal of HET-MOP-2 with the inset showing the atomic percentage of Rh(II) and Cu(II) ions.

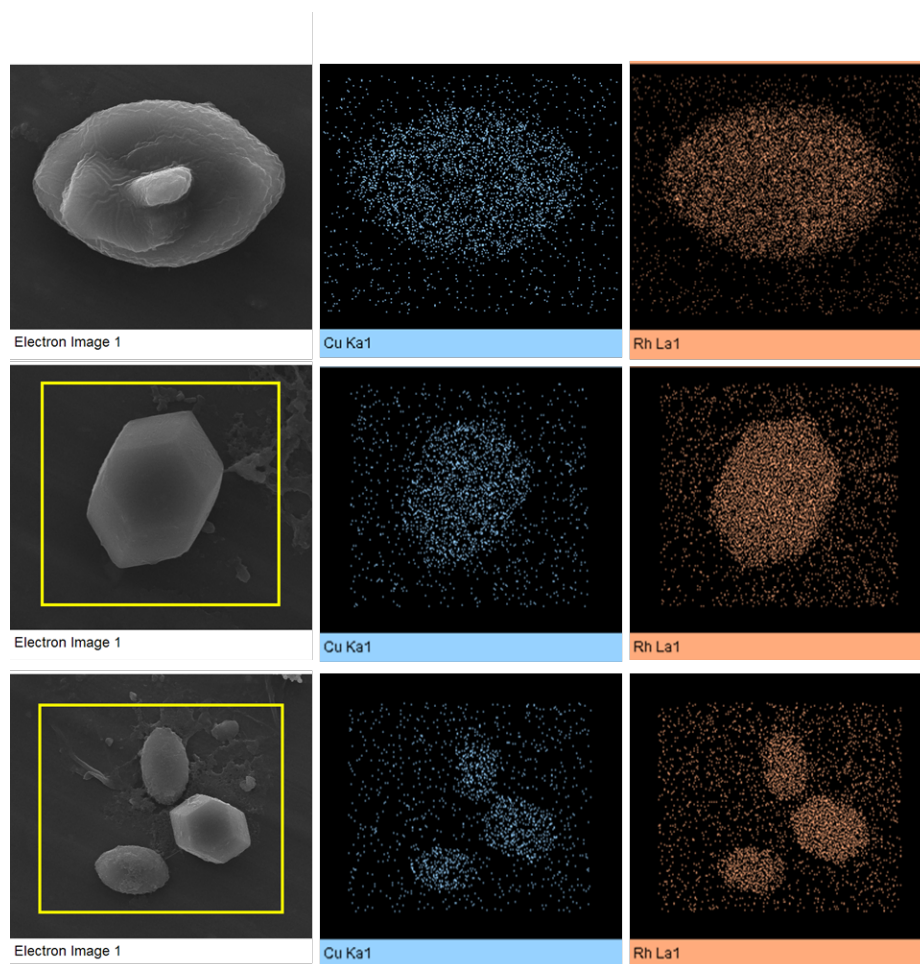


Figure S26. EDX Mapping of three different single crystals of HET-MOP-2.

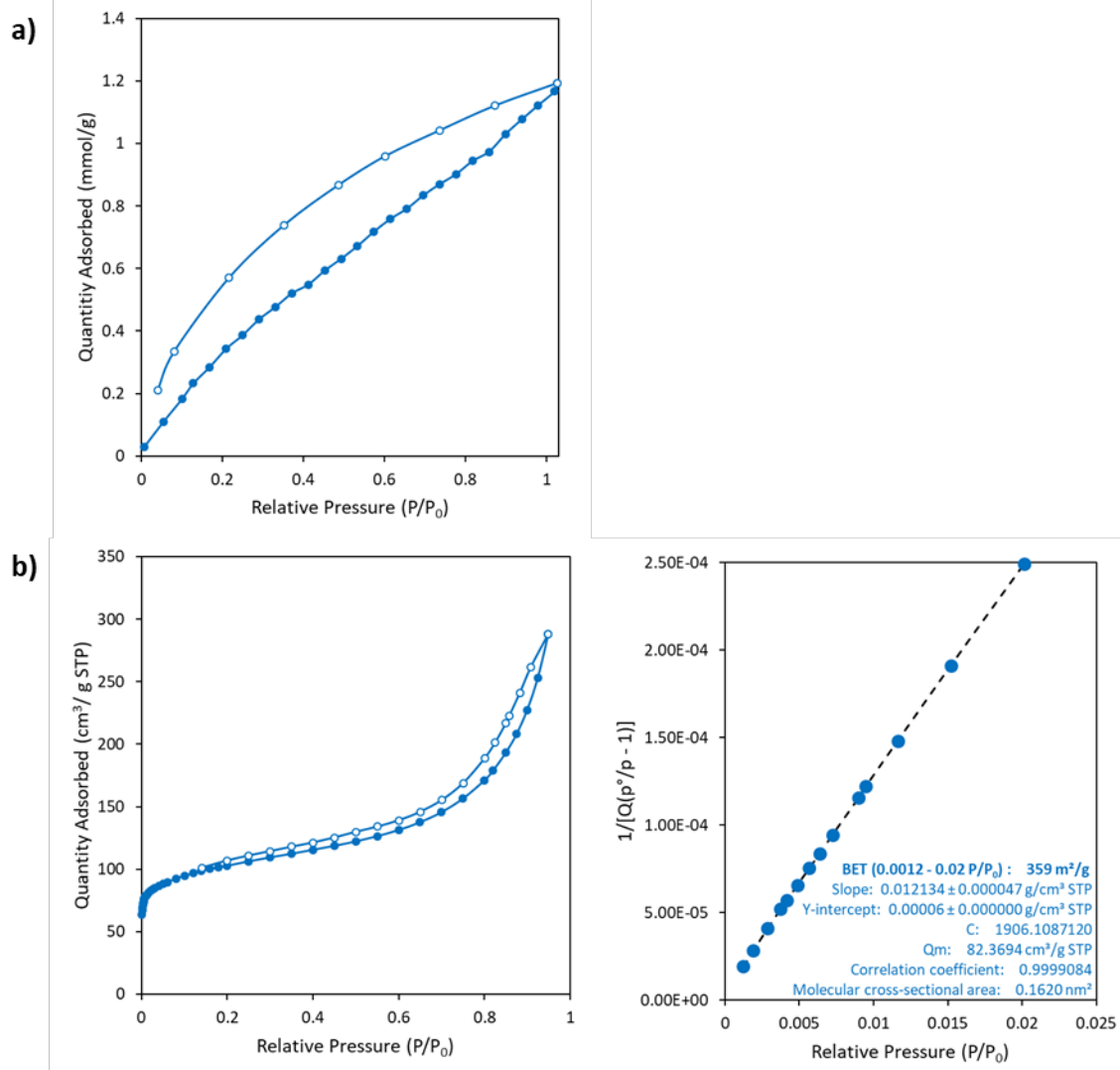


Figure S27. Gas adsorption isotherms for a) CO₂ at 298 K and b) N₂ at 77 K of HET-MOP-2. Solid spheres depict adsorption and empty spheres shows desorption.

S6. Characterization of HET-MOP-3

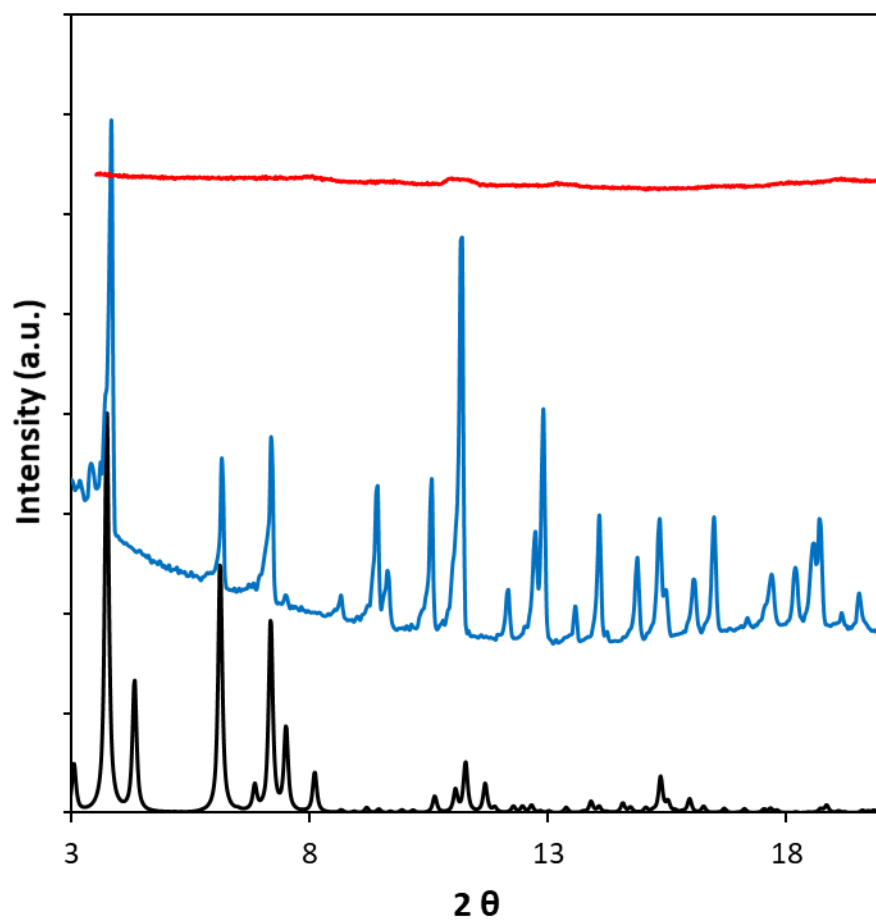


Figure S28. Simulated (black) and experimental (blue) powder-XRD diffractograms of HET-MOP-3. In red, PXRD of activated HET-MOP-3 for the adsorption measurements

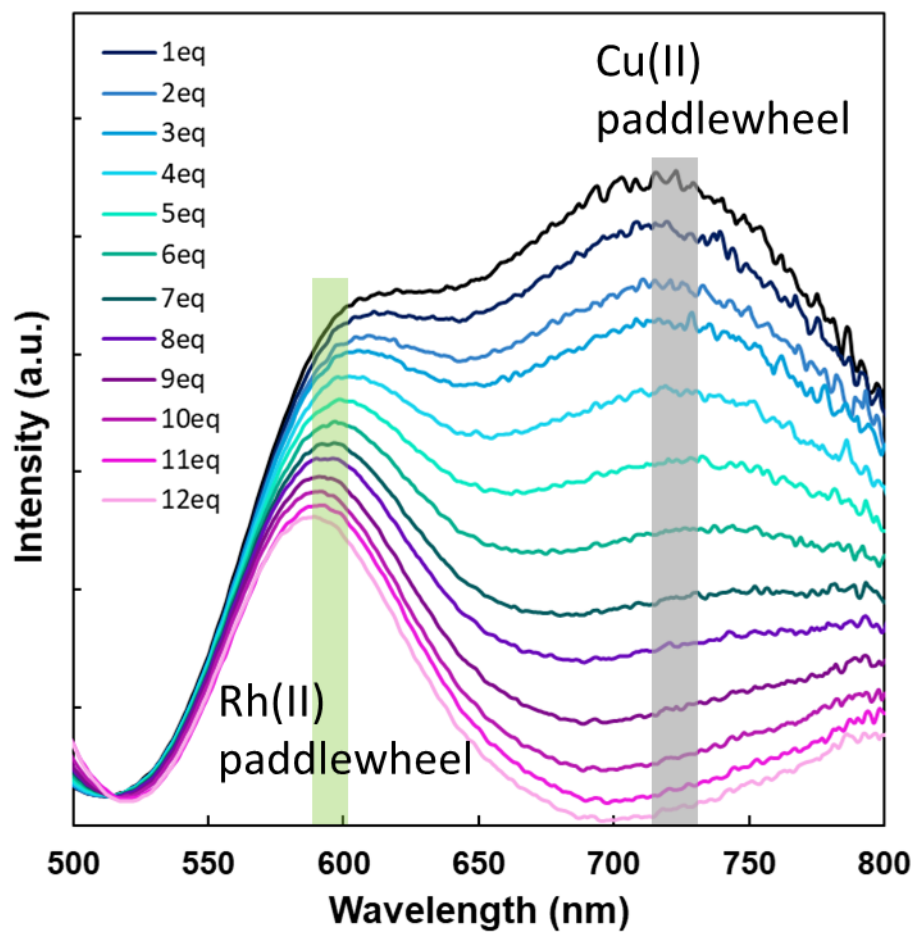


Figure S29. UV/Vis spectra of the disassembly of HET-MOP-3 with increasing amount of HCl (0.1 M) from 1 eq. to 12 eq. at room temperature.

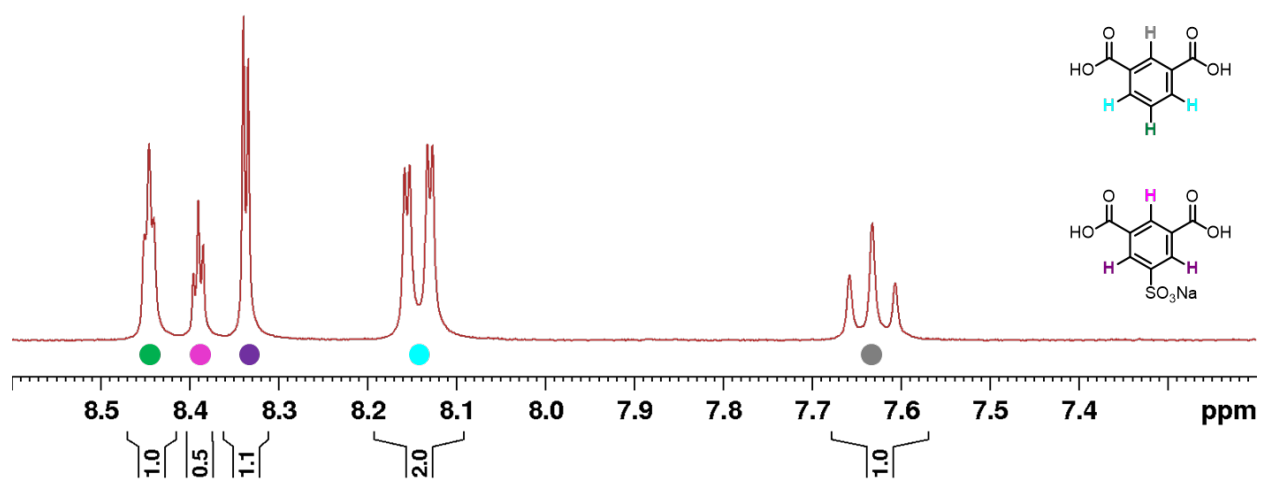


Figure S30. ^1H NMR spectrum (300 MHz, DMSO-d_6) of the acidic disassembly at 100 °C of HET-MOP-3, showing the appearance of the signals ascribed to free $\text{NaSO}_3\text{-bdc}$ and bdc .

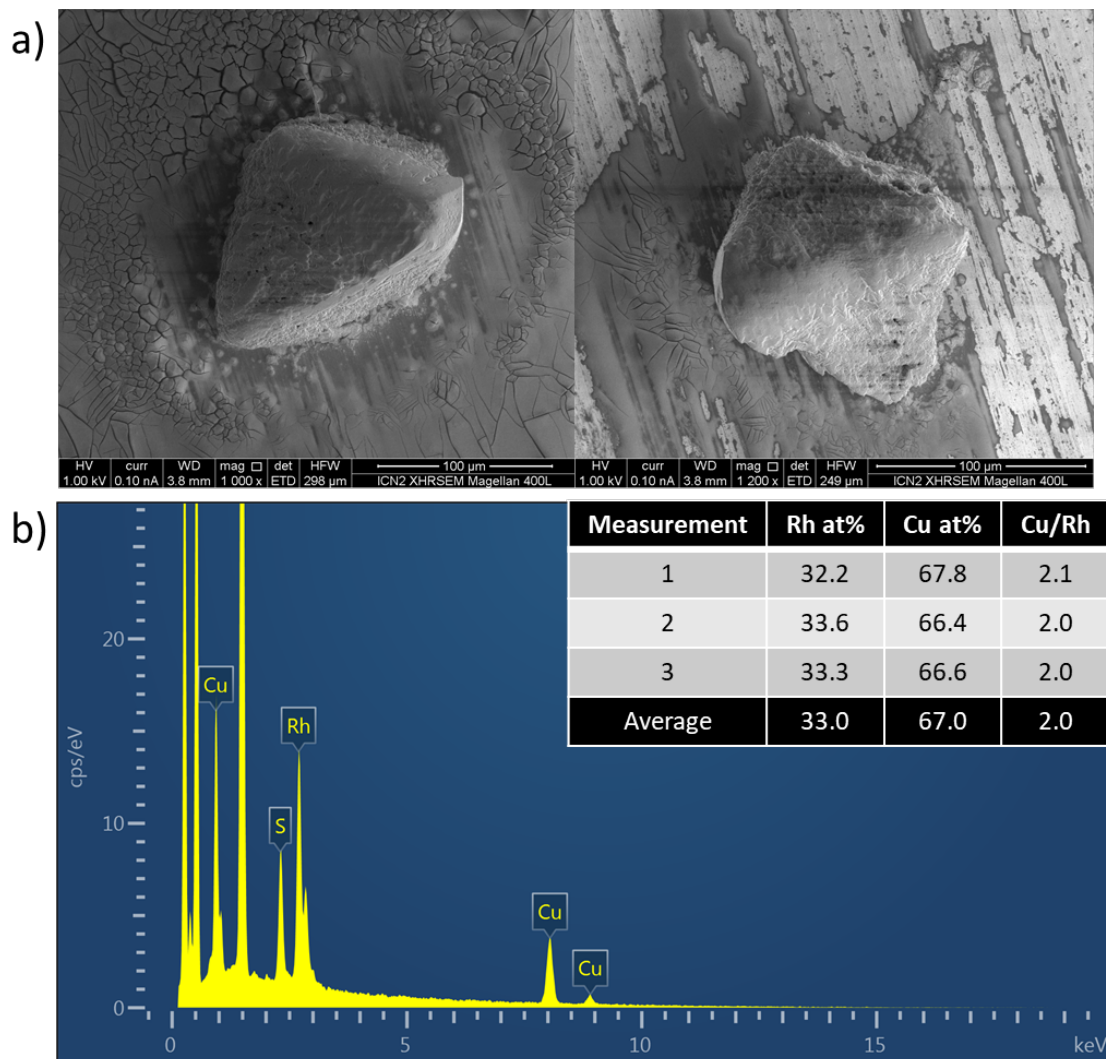


Figure S31. a) High resolution SEM images of two single crystal of HET-MOP-3. b) Corresponding EDX data of a single crystal of HET-MOP-3 with the inset showing the atomic percentage of Rh(II) and Cu(II) ions.

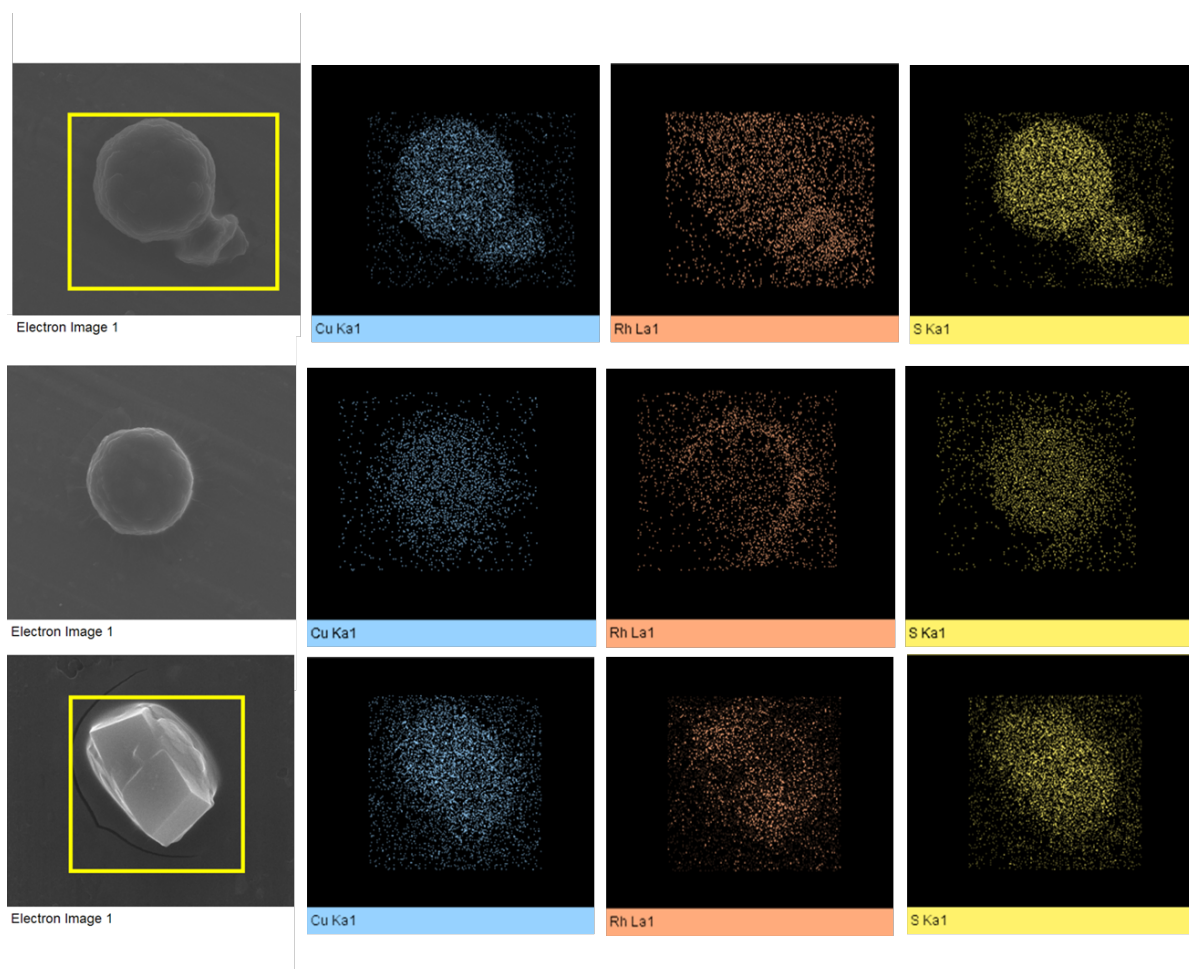


Figure S32. EDX Mapping of three different single crystals of HET-MOP-3.

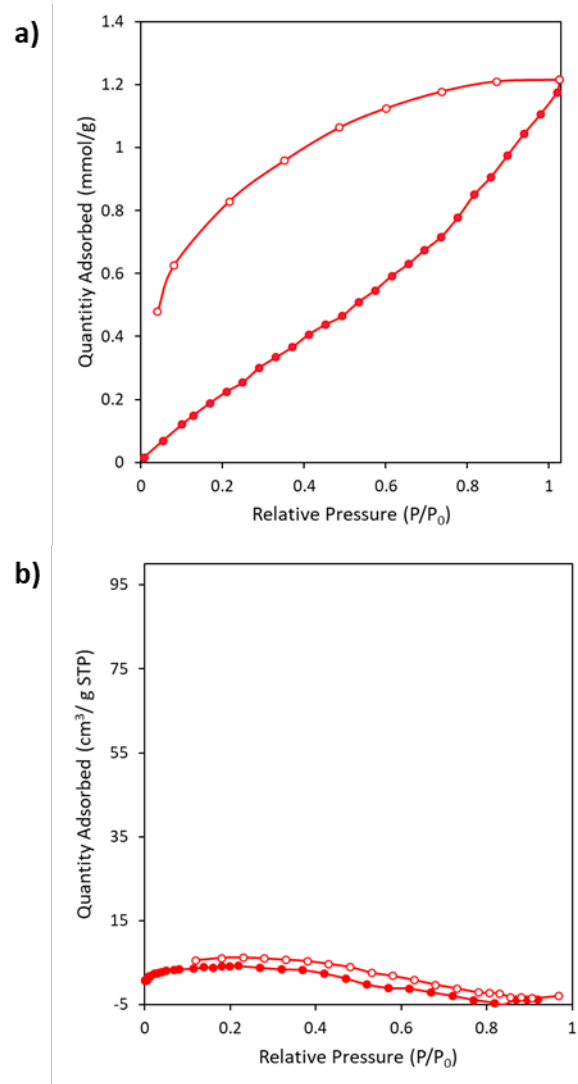


Figure S33. Gas adsorption isotherms of a) CO₂ at 298 K and b) N₂ at 77 K of HET-MOP-3. Solid spheres depict adsorption and empty spheres shows desorption.